POLITECNICO DI TORINO

Department of Structural, Geotechnical, and Building Engineering

Master's degree in Civil Engineering

Thesis of Master of Science

Calculation of residual prestress levels on beam bridge elements using a non-destructive and a destructive method.

Tutors

Prof. Francesco Tondolo

Eng. Pierclaudio Savino

Candidate

Emmanuel Gómez Restrepo

November 2022.

Abstract

Residual prestress levels are a crucial parameter when assessing the state of existing prestressed concrete elements on bridges. Large deflections and cracking may be caused by significant long-term prestress losses, affecting the bridge serviceability state and, in some cases, causing its collapse. Obtaining a reliable measurement of such parameters is usually a complicated task, as it often involves destructive testing of the bridge element. Researchers have developed and applied several destructive and non-destructive methods (e.g., crack moment, decompression load, strand cutting, exposed strand, drilled hole, and saw cuts). However, despite these advances, there is still no reliable technique, as each case is affected by multiple parameters such as materials, construction methodology, or maintenance.

This thesis aims to find a practical application for the assessment of residual prestresses, replicable for existing bridges. A non-destructive method and a destructive method are applied to six 50-year-old precast prestressed concrete beams with lengths of around 20 m. The tested beams are taken from the dismantled Corso Grosseto Viaduct in Turin, in the BRIDGE|50 research project scope. The applied methods are the "concrete-relax" method which measures the strains generated by completely isolating a small concrete block in the bottom flange of a PC beam by saw-cutting it; and the "strand-cutting" method which consists in completely exposing a prestressed strand, which is cut to obtain its prestressing stress. In the end, the purpose of this thesis is to bring an objective comparison between the results obtained using the non-destructive and destructive methods.

A mis padres, por el apoyo incondicional, la confianza y la paciencia,
en honor a ustedes hoy soy un poco de ambos.
A Sebastián por enseñarme siempre lo verdaderamente importante e inspirarme.
Los Amo.

A mis amigos y compañeros por apoyarme y acompañarme en este proceso.
A todos mis maestros por sus enseñanzas.
A la Universidad de Antioquia que es mi segundo hogar y al Politecnico di Torino
por abrirme sus puertas.

Index

List of figures.

List of tables.

1. Introduction

Throughout history, bridges have been the quintessential communication structure for surrounding places where physical interaction is limited or restricted by any natural obstacles such as valleys or rivers, or man-made structures such as roads, rail lines, or constructions. Bridge construction techniques through history vary along different cultures, and they have evolved along with humankind and our need for improving and evolving the way we transport. From the prehistoric era, stone designs were already used to cross environmental obstacles; Asian and American cultures built rope bridges with the available wood and plants; and the ancient Romans developed arc bridges made of masonry and concrete, many of which are still on feet today (Maya Vélez et al., 2019). In the last century, the improvement and development of construction materials and techniques have enhanced the possibilities. Prestressed concrete is one of the most revolutionary modern technologies, as it has allowed the building of higher-span bridges. However, as with any other concrete structures, prestressed concrete structures can be highly affected by deterioration (Hamilton et al., 2005).

The aging and deterioration process's impact on reinforced concrete and prestressed concrete structures can be exceptionally high. For most structures, -especially bridges- built in the 50s, 60s, and 70s, when exposed to aggressive environments, structural members made of concrete and reinforced with regular or prestressing steel showcase serious deterioration problems such as steel corrosion over time. Several recent studies and events have made engineers aware of how civil structures, particularly bridges and transportation infrastructure, are susceptible to the detrimental impact of aging, fatigue, and deterioration processes. These alarms warn about the substantial underinvestment in most developed countries for such structure's retrofitting, as in Italy particularly; a massive stock of bridges and infrastructures facilities are rapidly approaching the end of their service life as they were built over the past 50 years, bringing a large scale of needed repair or

replacement interventions which represents a key obstacle to nations development (Biondini, et al., 2021).

As a response to these needs in the Italian-specific context, the BRIDGE|50 research project was established recently; said project investigates a 50-year-old bridge (Corso Grosseto Viaduct) structural performance through an extensive campaign of non-destructive and destructive experimental tests. The works and tests in this thesis are performed as a side and complementary research to the BRIDGE|50 project. It is expected that the results obtained from BRIDGE|50 contribute to a contemporary approach to a life-cycle design of bridges, as well as to the improvement of the existing infrastructure system's safety, management, and maintenance.

Figure 1. (a) Corso Grosseto viaduct (Turin). (b) Bridge deconstruction process
(Anghileri, Biondini, et al., 2021).

Prestressed concrete is today one of the popular techniques used in bridge construction. The first applications of prestressing systems can be back-traced to the first half of the 20th century. Currently, it is used widely for many applications that go from small members, such as railway sleepers, to more critical structures, such as bridge girders in our case study. Prestress force is usually reported as the main factor on which the serviceability and safety of Prestressed Concrete (PC) structures rely (Bonopera et al., 2020). In bridges, prestressing methods are used mainly to reduce deflections and partially counterbalance dead and live loads' effects.

Serious inconveniences and damages can be caused by an extreme loss of prestressing forces, like deflections, or the jeopardizing of the performance of large-span PC girders by indicating cracking phenomena (Bruce et al., 2008). Then, knowing the prestress losses becomes an essential part of the assessment of in-service bridges. For this purpose, multiple studies applying diverse methods and techniques to determine the prestress loss have been performed, as well as some studies of actual bridges that failed due to the loss of prestressing force in their members.

Woodward (1989) described the investigation of a single-span, segmental post-tensioned concrete bridge that collapsed in South Wales. The bridge was built in 1953 and collapsed in December 1985. The investigators concluded that the bridge deteriorated due to corrosion of the prestressed steel tendons, which passed through the segmental joints.

Shenoy & Frantz (1991) Tested two 27-year-old precast, prestressed concrete box beams. The beams were removed from a deteriorated single-span, multi-beam bridge and subjected to structural load tests. Prestress losses were measured experimentally using the cracking moment method and the theoretical PCI (Precast/Prestressed Concrete Institute) method. Maximum prestress losses were much less than predicted.

A special report by the PCI journal named "Corrosion of Prestressing Steels and Its Mitigation" (Podolny, 1992). Motivated by the evidence of severe corrosion damage in prestressed concrete structures and bridges in many countries and the increasing concern of engineers regarding the corrosion of prestressing tendons and the impact of long-term service life. The paper discusses the magnitude of the problem and describes different corrosion mechanisms and some methodologies to prevent it regarding prestressing steels.

A non-destructive prestress loss evaluation technique was implemented by Azizinamini et al., (1996); the proposed method, and the crack reopening test, were performed on a 25-year-old prestressed concrete girder. The proposed method is based on the stress state around a small cylindrical hole drilled at the bottom flange of a prestressed girder. The authors ensure that the technique overcomes some of the shortcomings associated with other strain/displacement-based prestress evaluation methods.

Halsey & Miller (1996) Performed destructive testing of two specimens from a 40-year-old inverted T-beam prestressed concrete bridge. The authors applied three methods to measure prestress loss values: cracking moment, crack reopening, and strand cutting. They found a reasonable agreement comparing the measured values with the AASHTO Code prestress loss estimates. Similarly, several methods were used to test the remaining level of prestress in 2 full-scale, precast pretensioned box girders (Labia et al., 1997); The authors performed a complete testing program. A good agreement was concluded between the code predicted and measured ultimate load. But a significant difference between ductility and prestressed loss from code predictions.
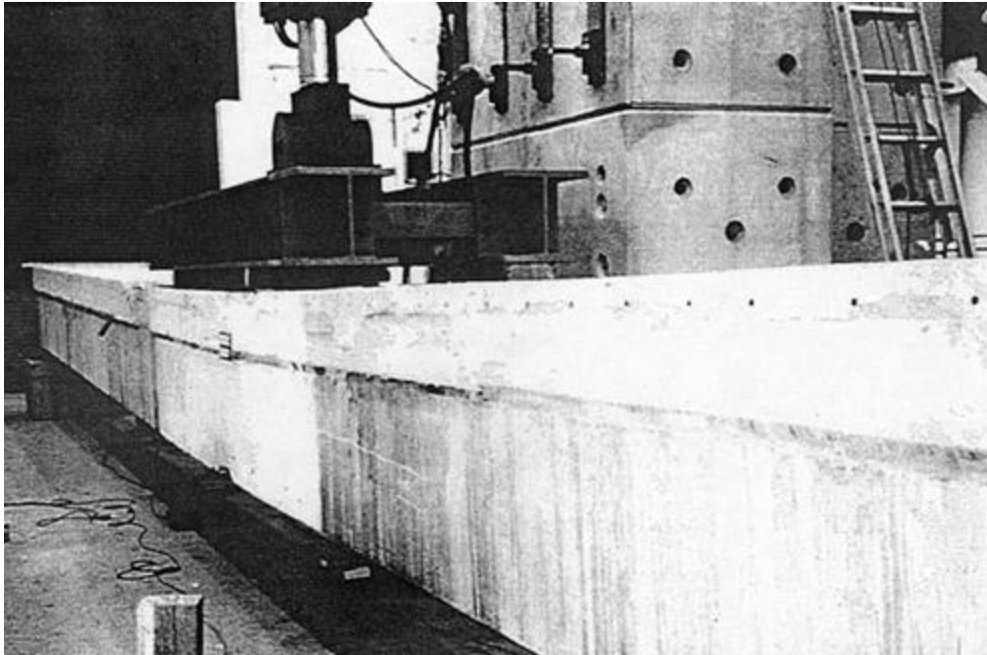
Figure 2. The general test set up for the experiments conducted by (Labia et al., 1997).

Civjan et al. (1998) Developed a prototype instrument "to estimate stress levels in exposed prestressed strands in existing members." The stress level can be determined by applying a lateral force on an exposed strand and measuring the resulting displacement. The instrument must be calibrated for a respective strand type. Strand forces were consistently estimated to be within 10% of the actual load.

A comparison of field-measured prestress concrete losses vs. design code estimates is performed by Onyemelukwe & Mills (2003). In this study, an actual bridge is instrumented with embedded vibrating wire strain gages during construction. The axial strain data is used to determine the girder's time-dependent prestress loss variation and distribution. Comparing the measured loss with the estimates of the PCI and the AASHTO indicates that the field-measured prestress loss is non-uniform across the girder depth as opposed to a uniform distribution assumed in most codes.

B. M. Kukay (2008) researched destructive and non-destructive techniques development to determine the residual tendon stress directly in prestressed girders. The author embodies a "three-prong approach" to determine residual prestress

force. (1) In new bridges, outfitting girders with instrumentation, (2) destructive techniques for already constructed bridges, and (3) non-destructive techniques development for bridges intended to be kept in service. Later, in 2010, B. Kukay et al. presented a paper where they tested some bridge girders that had been in service for around 40 years, implementing a new non-destructive technique. On average, the non-destructive test results were within 94% of the results based on cracking tests.

A comparison of methods for experimentally determining the prestress losses in pretensioned prestressed concrete girders was performed by (Baran et al., 2015). In the paper, the effective prestressing force was determined by three methods: (1) using vibrating wire strain gages embedded in the girders during fabrication; (2) load testing to determine flexural cracking and crack reopening loads and then back calculating the losses; and (3) exposing a length of strand attaching resistance strain gauges on the strands, and flame-cutting the strands. The experimentally obtained values were lower than the predicted values using PCI Committee and AASHTO LRFD methodologies.

Higgs et al. (2015) performed a study aiming to quantify the behavior of precast, prestressed-concrete bridge girders made with high-strength concrete. The study tested four girders. Each girder was subjected to a flexural cracking test to determine a prestress loss of 22% after approximately seven years of service life.

In an extensive experimental study, 30 full-scale precast, pretensioned bridge girders were constructed and instrumented. Garber et al. (2015) Used several precast beam fabrication plants to investigate the influence of different concrete materials and construction techniques. Prestress losses were measured using vibrating wire gauges (VWG) embedded in the specimens. The measured short and long-term prestress losses were compared to the ones obtained with several estimation procedures suggested by ACI Committee 423. A different paper by Garber et al. (2016) presents a new prestress loss estimation procedure that can be used for both

time-dependent and final prestress loss estimation; the authors describe the procedure as simple to use and precise.

Two existing non-destructive and destructive approaches to determine residual prestress levels were applied to girders from a 55-year-old bridge in Sweden (Bagge et al., 2017). The focus of the program, pursuing practical applications, was a non-destructive methodology combining experimental data and finite element modeling to obtain residual prestress force. They obtained that determined residual prestress forces were generally higher than theoretically based estimates, which accounted for friction and time-depending losses in a prestressing system.

Frizzarin et al. (2019) Performed an experimental campaign on six PC beams and different levels of prestressing. Static tests were carried out until obtaining beam failure. On each load step of the test, several non-destructive tests were carried out, namely dynamic free vibration tests and ultrasonic tests.

A state-of-the-art review of important worldwide research works on determining prestress losses was performed by Bonopera et al. (2020). The authors primarily focused their attention on a static non-destructive method and elaborated a comparison with dynamic ones. Concluding that "a variation in prestress force does not significantly affect the vibration response of such PC girders."

As seen in the previous paragraphs, there is a significant quantity of research projects aiming to find and describe ways of estimating the residual concrete prestress levels on PC members. However, there is still not an entirely reliable method to be applied to members still in service. The finding of such a method would imply an important advance as the residual prestress levels are an essential parameter to evaluate the element's current state and, based on it, make decisions concerning its future use, maintenance, or immediate dismantlement (Rogers et al., 2012).

This thesis aims to find the residual prestress levels on six 50-year-old precast

prestressed concrete 20 m beam elements taken from the Corso Grosseto viaduct in Turin. For this mean, two different kinds of tests are performed, the first one is the non-destructive "concrete relax" test, this test looks into isolating a 7 cm wide concrete block in the bottom flange of the elements, applying a similar principle to the "saw-cut" test described on (Bagge et al., 2017; B. Kukay et al., 2010), with some practical differences that are described later in the text. The second test is a destructive rebar-cutting test performed in the same spots previously intervened.

Figure 3. (a & b) Strand cuts. (c) Concrete relax (saw-cuts) test.

The small dimensions of the cut concrete block allow later intervention to return the element to its original state, and it does not involve altering any common or prestressed reinforcement element. It does not significantly impact the structural behavior of the beam; such reasons, along with its simplicity and low economic cost, make it an ideal alternative in the evaluation of different typologies of prestressed

bridge elements. In the case of a reasonable accuracy of the "concrete relax" method result, it can open the door to further research for this kind of test, as it can be an essential tool in the future assessment of in-service bridges.

The structural outline of this document initiates with a description of several corrosion processes in steel strands; then, some tests for the evaluation of residual prestress levels (e.g., crack moment, decompression load, strand cutting, exposed strand, drilled hole, and saw cuts) are described. After it, it is described the beam and elements' geometry and characteristics; being followed by the performed tests' detailed description and the test program. The performed computations and obtained results analysis are presented in the following section. In the end, some conclusions are given, and some advice and recommendations to take into account in future works.

2. Assessment of existing bridges: concrete and steel degradation and assessment on bridges.

Different forms of concrete deterioration have been a particular topic of concern and struggle for such material development and usage in civil infrastructures from its first application back in the 19th century of traditional reinforced concrete, and the introduction of prestressed concrete in the 20th century (Lau & Lasa, 2016; Podolny, 1992). Corrosion of steel components like reinforcement and tendons constitutes the leading cause of deterioration and, in many cases, even failure. For many years, it was wrongly assumed the adequate corrosion resistances of reinforcements on traditional and prestressed concrete structures, due to the demonstrated corrosion-inhibiting properties of portland cement for the steel embedded in it. For prestressed concrete elements, this resistance was believed to be even higher by the "crack-free" configuration of such structures due to prestressing (Podolny, 1992). Moreover, concrete is still susceptible to its usual and known causes of degradation (de Schutter, 2013).

Prestressing techniques for concrete bridges are diverse and are widely used for bridge superstructure and substructure elements (Lau & Lasa, 2016). Several decades of experience with the technique, and continued improvements and innovations in its application, have further helped garner acceptance of prestressed concrete by bridge engineers and owners. In contrast to the advantages and good general use of prestressed concrete for over 60 years, documented durability problems and component failures in arguably isolated cases continue to illustrate difficulties in bridge applications. Unfortunately, corrosion concerns over the steel

components of prestressed concrete bridges have persisted. Prestressed bridge systems are complicated, and many structural, construction, material, and environmental factors can be involved in corrosion development. The ACI (American Concrete Institute) also notices this lack of knowledge on the topic; as (Hamilton et al., 2005) state, for prestressed concrete structures, corrosion is not as well documented as in non-prestressed concrete structures. Corrosion of these elements appears to be delimited to specific circumstances, including construction details, improper design, and construction practices. The potential for widespread problems still exists, and it is imperative to protect steel elements in corrosion promoters contaminated environments.

Figure 4. Prestressed corroded tendons at the end of a PC beam.

The corrosion of steel tendons in prestressed concrete structures can bring up more severe consequences than in conventional reinforced concrete structures (Hamilton et al., 2005; Podolny, 1992), as the prestressed tendons have a relatively small area of the cross-section under higher magnitudes of stress. There is a more significant susceptibility to developing a brittle fracture caused by stress corrosion or hydrogen embrittlement. Corrosion-related fractures can lead to bridge collapse without warning, as has been registered before (Parrondo Rodriguez, 2017; Woodward, 1989).

Figure 5. Collapsed M-527 bridge, Madrid community, Spain (Parrondo Rodriguez, 2017).

Figure 6. Ynys-y-Gwas bridge after collapse, West Glamorgan, UK (Woodward, 1989).

Moreover, (Podolny, 1992) holds that from 242 cases of prestressed steel corrosion damage registered in the literature from 1951 to 1979, 13% were bridges, and the main causes of corrosion were deficiencies in the protection systems and exposure to humid environments. Podolny also states that by the time (1992) there was already a discernible trend of corrosion incidents reports, which three factors can partially explain: (1) The population of prestressed concrete structures age is increasing, (2) the increase in the use of deicing salts from the 90's, and (3) More structures

constructed close to harsh environments.

2.1. Prestressed bridges corrosion mechanisms overview.

Corrosion is the term that describes a metal deterioration process due to a chemical or electrochemical reaction with its environment. This thesis will not thoroughly discuss the complete processes and causes of corrosion in prestressed steel elements as it is not the main focus of this work; however, it will present a synopsis of the most essential corrosion mechanism in prestressed bridges.

Prestressed concrete bridges present many factors that can produce a variety of corrosion mechanisms; such factors involve prestressing techniques, structural components, construction procedures, deficiencies in building materials, and natural and service conditions. (Lau & Lasa, 2016). In both pretensioned concrete, and bonded post-tensioned concrete, prestressing steel is encapsulated in cementitious grout or concrete, generally resulting in similar corrosion processes as those presented in conventional reinforced concrete. However, the structural implications and damage may be more severe than in the last-mentioned ones (Hamilton et al., 2005; Lau & Lasa, 2016).

Some of the main factors complicating the corrosion system's wellbeing could be the use of high-strength steel and multiwire strand, the presence of a prestress force, the presence of segment joints, the use of cementitious grout, and the presence of other building materials further complicate the system (Lau & Lasa, 2016). Also, the three previously cited works (Hamilton et al., 2005; Lau & Lasa, 2016; Podolny, 1992) coincide, stating that in specific environments it can be a concern the possible occurrence of hydrogen embrittlement and stress-corrosion cracking, both being brittle mechanisms.

Figure 7. (a) Broken out strands with uniform corrosion; (b) Individual wires with pitting damage, from (Rogers et al., 2012).

Stress Corrosion Cracking (SCC).

Stress corrosion cracking refers to cracking caused by the simultaneous presence of tensile stress and a specific corrosive medium (Fontana, 1987; Hamilton et al., 2005); it can be either an applied or a residual tensile stress.

SCC is a type of highly localized corrosion, which, in combination with the tensile stresses, causes cracking; this phenomenon can occur at stresses within the range of design for which it must be specially considered. The corrosion process produces a discontinuity on the metal surface in the form of a pit, generating stress raising in the respective point (Podolny, 1992).

The generation of stress corrosion cracks at the pit's base has often been observed after the crack initiation. A large concentration of stresses at the crack's tip produces a crack propagation effect. The crack propagation can be intergranular or transgranular, that is, along grain boundaries or on slip planes within the crystal lattice (through the grains). The crack can eventually generate enough cross-section reduction to trigger a brittle failure (Fontana, 1987; Hamilton et al., 2005; Podolny, 1992).

Hydrogen Embrittlement (HE)

Hydrogen embrittlement is defined as the reduction in ductility due to the absorption of atomic hydrogen into the metal lattice, where it recombines into hydrogen molecules, producing an internal pressure in the element (Fontana, 1987; Podolny, 1992). HE occurs only with the absorption of hydrogen atoms because the molecule is too large to penetrate the steel's crystalline structure; there is no need for the material to be stressed for HE to occur, unlike SCC (Hamilton et al., 2005).

The atomic hydrogen may be formed by the corrosion process itself or as a result of some manufacturing operation, such as pickling. For instance, hydrogen embrittlement can occur when the tendon is just resting in the duct previously from the stressing process and grouting, then, when the tendon is prestressed, the HE-produced corrosion becomes apparent, and the tendon fails (Fontana, 1987; Hamilton et al., 2005).

The internal pressure caused by the hydrogen molecules develops tensile stresses initiating cracking phenomena on the metal or in combination with critical external tensile stresses. Atomic hydrogen may enter the metal over extended periods, meaning it can be a long-term developed phenomenon. Rupture due to hydrogen embrittlement has occurred several years after installation. (Podolny, 1992).

Both types of failure (SCC and HE) occur by brittle fracture and may have the same appearance, that is, a little necking. In both, pitting or general corrosion may or may not be present, and a minimal associated elongation and reduction of the cross-sectional area occur before fracture.

Fretting Corrosion

Corrosion by fatigue fretting is a phenomenon that can affect prestressing

strand/wire used in post/tensioned applications. It occurs at the contact area between two materials and is manifested in surface wearing due to the vibration and slip to which two surfaces, in contact and under load, are subjected (Fontana, 1987; Hamilton et al., 2005; Podolny, 1992). For fretting corrosion to happen, it requires interface pressure and the presence of vibrating or cyclic relative motion of a magnitude high enough to produce a slip or deformation on the mating surfaces. According to (Fontana, 1987), the following three conditions must be satisfied in order for damage to be considered fretting corrosion (and not wear):

- The interface should be under load;
- A repeated small relative motion must occur between the two surfaces; and
- The load and relative motion on the interface should produce relative slip and deformation on the surface.

The relative motion required to produce fretting corrosion can be minimal (10^{-7} mm) according to ACI 222.2R-01 (Hamilton et al., 2005; Podolny, 1992). The relative motion of the surfaces causes wear and corrosion of the surfaces in the presence of oxygen, causing wear and corrosion at the interfaces.

In prestressing strands used in post-tensioned bridge girders, the process that causes fretting corrosion can also cause fatigue cracking. Strands are in close contact with each other inside the post-tensioning ducts; this contact, combined with cyclic loading, can lead to fatigue failures due to fretting (Hamilton et al., 2005).

2.2. Material Properties and Service Conditions

When it comes to material properties and service condition influence on corrosion of prestressing steel wire or strands, (Bruce et al., 2008) expose the following:

- Metal properties - have the most negligible influence on corrosion resistance;

- ▪ Concrete quality - especially the one surrounding the wire or strand, has a significant influence on corrosion resistance;
- ▪ Service conditions of the bridge - have the most significant influence on corrosion resistance.

Steel Properties

Steel properties are determined by the chemical composition and the thermal treatments applied to the metal. Elastic behavior and ductility at stress levels of loading, low relaxation of tension, resistance to stress corrosion cracking, and resistance to hydrogen embrittlement are important steel characteristics (Lau & Lasa, 2016). Moreover, high strength with high elongation are properties required for steel used in prestressing (Bruce et al., 2008).

Wires and strands used in prestress applications are usually made of high-carbon steel submitted to cold-work processes and thermal treatment to attain desired material characteristics. Due to the extra energy used in these processes to produce the higher yield strength, these steels have a lower corrosion resistance than steels used in standard reinforcement bars (Bruce et al., 2008; Lau & Lasa, 2016). However, for any prestressing steel used, its mechanical properties, composition, and the manufacturing process utilized to fabric the wire and strands should be optimized to provide good corrosion resistance. Prestressing wires and bars are made by one of the following four processes:

- ▪ hot-rolled stretched and stress-relieved bars,
- ▪ quenched and tempered martensitic wires/bars,
- ▪ cold-drawn, stress-relieved wires/strands, and
- ▪ cold-drawn wires

Due to their high carbon content, these high-strength steels are particularly

susceptible to hydrogen embrittlement (Fontana, 1987). This increase in carbon content, as well as other "poisonous" elements such as phosphorus, antimony, tin, sulfides, and arsenic that can be present in the grain boundaries, increase the amount of hydrogen entrapped in the steel lattice (Bruce et al., 2008).

Bruce et al. (2008) also point out three questions to be answered to determine if the nature of the prestressing steel in a particular bridge has contributed, or may contribute, significantly to an observed failure; these questions are:

- Was the same steel used in all beams on the bridge? If not, is the poor performance of one beam related to the wire product used?
- Did the failed steel comply with the design specifications for the bridge (i.e., was the correct steel used)? If not, the problem may be limited to this bridge or others built with the same product.
- Does the failed steel comply with the current specifications for prestressing wire? Moreover, from current knowledge, would we expect it to perform satisfactorily?

Concrete quality

Cement paste counts with high alkalinity, and its permeability is relatively low to moisture, oxygen, and chlorides; these properties typically protect the steel embedded in it. If concrete's cover alkalinity is reduced, corrosion on the steel will start. This alkalinity reduction can be provoked by carbonatation or chloride contamination (Bruce et al., 2008; de Schutter, 2013).

To safeguard prestressing steel from the entrance of moisture, oxygen, and chlorides, an adequate depth of cover and quality of concrete is fundamental (Bruce et al., 2008). A correct mix selection is essential, but even in the best concrete mix designs, the presence of cracks and voids will increase the permeability (de Schutter, 2013).

Another factor that can increase permeability and the possibility of significant corrosion cracking damage on steel is inadequate concrete compaction. Also, in the case of prestressing steel failure, a deeper concrete cover can reduce the risk of spalling and cracking, likely minimizing the danger of a strand or wire bursting out of the element (Bruce et al., 2008).

Service conditions

Most cases of prestressing corrosion reported in the literature are related to poor drainage of the bridge structure, causing the entrance of moisture and chloride (and not from concrete alkalinity carbonation) (Bruce et al., 2008). This poor drainage is caused by deficient design and poor or utterly null maintenance of features such as drains and joints.

Steel can be contaminated with chloride in diverse situations, e.g., before being cast into the concrete while being stored in marine environments, or it can be contaminated being already in service from extended exposure to seawater, sea spray, or deicing salts (Bruce et al., 2008). The highly localized corrosion pitting caused by chloride makes them a very particular problem; thus, localized corrosion can reduce the cross-section enough to provoke a steel failure under normal working loads (Fontana, 1987). The acidification of corrosion pits can cause hydrogen embrittlement, and corrosion can be promoted at lower chloride concentrations than for unstressed steel (Bruce et al., 2008; Fontana, 1987).

Corrosion can also be induced by stray currents coming from electrical or cathodically protected services. The fact that a stray electrical current may pass through the prestressing steel is frequently ignored or overlooked by designers; this current produces a potential difference between the concrete and steel and lead to the creation of electrochemical corrosion cells. In this case, it can be easily detected by its characteristic appearance (Bruce et al., 2008; Podolny, 1992). Structures

particularly vulnerable to this type of phenomenon are those associated with electrified rails or tramway systems, as well as those elements fully or partially embedded in the ground (e.g., bridge piers, footings, and piles, or bridges over sea bodies in which concrete and steel act compositely and seawater act as the electrolyte (Podolny, 1992).

A wire undergoing general corrosion can show a premature failure when overloading (Bruce et al., 2008). A ductile behavior mode is usually exhibited as a result of pure overloading. However, the relatively low ductility of prestressing steels may make it hard to identify this kind of failure.

Fatigue and fretting corrosion can also occur in partially prestressed elements or where the wire/strand bond is lost (Bruce et al., 2008).

Figure 8. Degradation and corrosion at support zones in the Corso Grosseto viaduct at different years of inspection. a) 2011, b) 2012, c) 2013, d) 2014 maintenance interventions, e) 2015 and f) 2016. (Savino et al., 2021)

31

2.3. Assessment of prestressed concrete elements.

Inspections of prestressed concrete structures may need to be more rigorous than inspections for traditional reinforced structures (Bruce et al., 2008; Hamilton et al., 2005); this is because of the higher risk involved and because visible corrosion signs in these special structures are often absent or are minimum. (Bruce et al., 2008) present a list of features that may serve as indicators of an increased likelihood of corrosion in prestressed elements; these are some of them:

- drainage of runoff over the surface;
- cracking, particularly if it is not expected from normal loading;
- insufficient depth of concrete cover, especially on surfaces exposed to runoff or chloride ingress;
- physical damage that reduces the adequate cover depth;
- leaking deck joints or other features of poor surface drainage that provide a source of moisture corrosion;
- inadequate concrete consolidation, as evidenced by surface voids;
- reduced alkalinity of concrete cover, particularly on surfaces exposed to runoff, and
- the elevated chloride ion content in cover concrete.

Original documentation of the structure can be helpful to detect possible risk factors. Design drawings, built drawings, and even ordering and purchase records of materials (Bruce et al., 2008)

Measurement of electrochemical corrosion potential (or "corrosion potential") has been used as an effective method to detect areas where corrosion is most likely to appear, although it may be difficult to distinguish between the risk of ordinary reinforcement and the risk of prestressing steel (Bruce et al., 2008; Hamilton et al., 2005). Field evaluation of prestressing steel corrosion in concrete structures is very similar to the evaluation of embedded mild reinforcing steel in concrete (Hamilton et al., 2005). Although there are similarities between the evaluation of both systems,

there are also essential variations and additions.

It is imperative to verify the extent and magnitude of any corrosion-induced damage to assess the effects of corrosion on a structure's capacity or serviceability, e.g., wire section loss, fracture, or concrete damage (spalling or delamination) (Hamilton et al., 2005).

Moreover, the ACI 222.2R-01 states that there are additional distinctions between pretensioned-system and post-tensioned system evaluations. Here was presented a summary of the methods and differences; detailed information can be found in the cited article.

Pretensioned systems:

As in mild reinforcing, the prestressed steel is bonded to the concrete, that is, in intimate contact. Hence, the pretensioned steel system's field evaluation is similar to a typical mild reinforcement for a concrete member corrosion evaluation. However, there are important distinctions between pretensioned and traditional reinforced concrete systems. Its evaluation methods can be classified as follows (Hamilton et al., 2005):

Electrical evaluation methods: These systems are not electrically isolated from the concrete, as can be the case with post-pensioned systems. Electrically evaluation methods developed initially for mild reinforcement corrosion evaluation can be used, for example, half-cell corrosion potentials and polarization resistance.

Material analysis: Material analysis may be focused on assessing the following three characteristics: (a) Chloride-ion content, (b) Carbonatation, and (c) chloride permeability.

Post-tensioned systems:

Evaluation of these systems differs significantly from the evaluation of pretensioned systems due to the configuration of such systems. Post-tensioned systems are composed of high-strength wire or strands contained within a duct (the duct is usually made of metal, plastic, or paper), which is encased by the concrete of the member; the duct is typically filled with cement, grout, grease, or petroleum wax that provide corrosion protection for the steel. Grout also fulfills a bonding function between tendons and the rest of the structure; when there is no grouting, tendons are considered unbonded; in some cases, there are also tendons that are external to the structure. Post-tensioned system assessment can be divided into two parts:

Evaluation of anchorages: An effective loss of the entire tendon can be considered after an anchor is completely damaged; this makes anchorages a critical component. In unbonded post-tensioned systems, corrosion evaluation of anchorages is essential, although it should also be paid attention to in bonded tendon systems (Hamilton et al., 2005). Anchorage evaluation may consist of a visual inspection, as the anchor is cast into the concrete without blockouts in order to provide access to the anchor for future stressing, and a material analysis of the anchor itself and the materials in its surroundings.
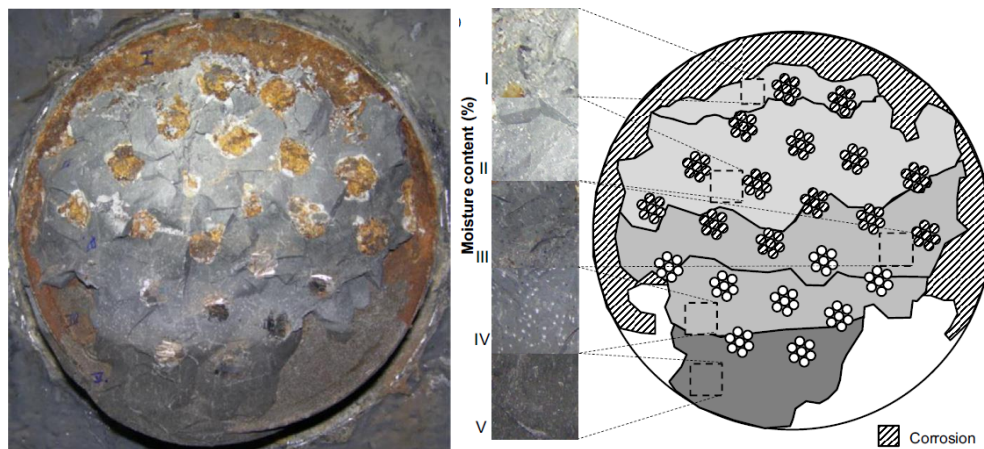
Figure 9. Deficient grout and corrosion at an anchor cap (Lau & Lasa, 2016).

Evaluation of tendons (unbonded): Methods usually employed for prestressed systems, such as remote electrical methods like half-cell potentials and polarization resistances, cannot be used on unbounded systems. The most common evaluation methods for this kind of system are invasive probing or the complete removal and examination of an entire tendon of the structure.

Evaluation of tendons (bonded): The duct and the cementitious grout generate a corrosion protection barrier for bonded tendons. The grout plays an essential role in this type of system; the tendon's susceptibility to corrosion is highly incremented if there is not a complete filling of the tendon ducts, if there is an absence of grout or if the grout is of poor quality. The evaluation of bonded tendon systems can be performed following the subsequent activities: (a) location of the tendon duct, (b) non-destructive evaluation of grouting, (c) non-destructive evaluation of tendon damage, and in case it is necessary, (d) non-destructive evaluation of tendon damage.
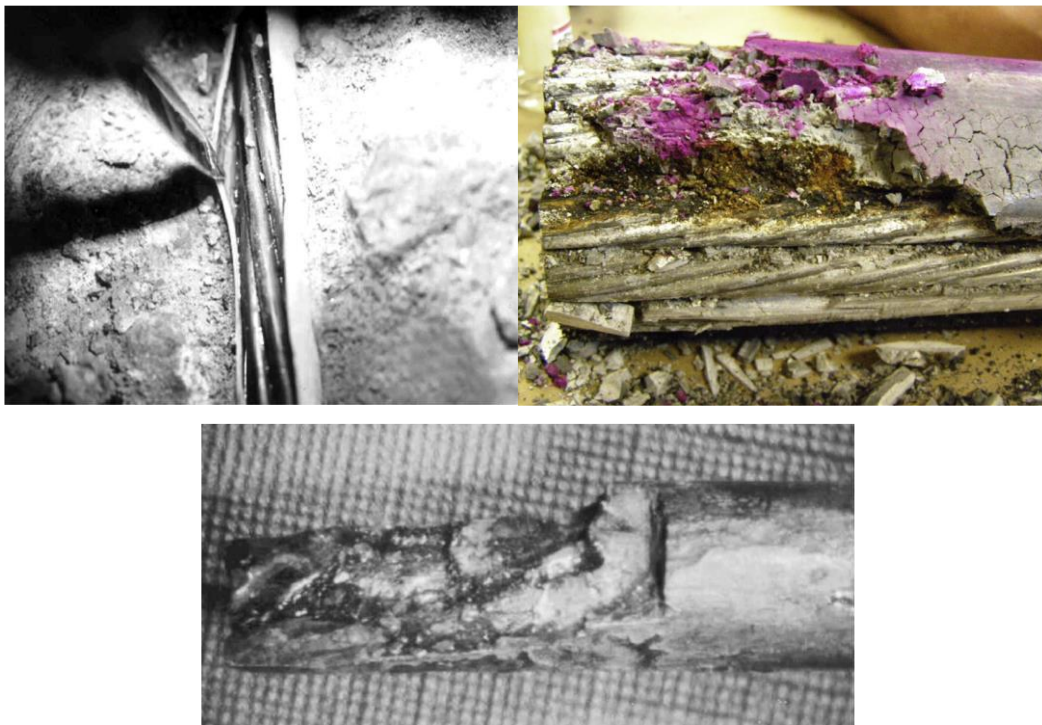
Figure 10. (a) In-place examination of an unbounded tendon, (b) corrosion of a strand embedded on deficient grout, (c) Brittle wire fracture. (Hamilton et al., 2005; Lau & Lasa, 2016).

3. Residual prestress assessment.

The decision of whether to repair or substitute a damaged prestressed concrete bridge girder can be challenging when a reliable estimation of prestress remaining in the strands is not available (Civjan et al., 1998). Accurate determination of residual prestress forces is essential in assessments of existing prestressed concrete bridges because they strongly influence the element's responses and capacities at serviceability and ultimate limit states. In addition to stiffening, prestressing reduces exposure and thus increases the resistance of such structures in aggressive environments by preventing cracks or limiting their growth. (Bagge et al., 2017).

Most transportation departments in the United States are uncertain about repairing girders with exposed strands or extensive concrete damage and prefer replacing the damaged girder. Such replacements are costly and time-consuming. There is a need for a more accurate damage evaluation method so that the integrity and safety of a repaired girder can be restored with confidence (Civjan et al., 1998). If the extent of damage or strand stress levels can be determined inexpensively and reliably (within 10 percent), repairs to a girder can then be designed to restore the original strength (Civjan et al., 1998).

In order to quantify the prestress forces in a concrete member theoretically, parameters influencing the prestress losses must be considered. Generally, the losses can be classified as pre-transfer or post-transfer, depending on whether they occur before or after prestress force is transferred to concrete. Losses due to friction and elastic shortening of concrete are considered pre-transfer losses. In contrast, losses due to slippage, concrete shrinkage and creep, and steel relaxation are post-transfer losses. (Bagge et al., 2017)

3.1. Destructive methods

Crack moment

In this type of destructive test, the external load causing the apparition of the first crack in a prestressed member is determined and used to calculate the prestress force (Bagge et al., 2017). Several techniques can be used for this, but the results may be inaccurate due to the existing uncertainties about the tested member tensile properties.

In 1991 Shenoy & Frantz determined experimentally the prestress force in two 27-year-old prestressed concrete box beams considering a cracked moment-based method. Once determined the crack opening load corresponds to the instant of the first crack opening, the prestress force can be calculated by statics. The bending moment due to dead load and applied load should be taken into account.
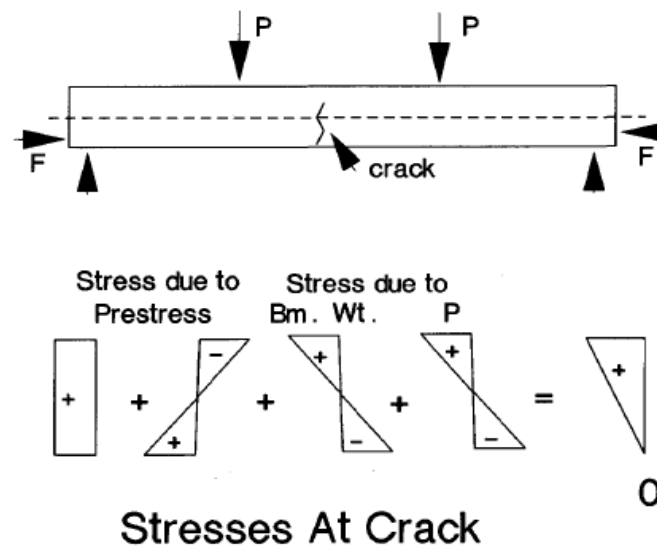
Figure 11. Static scheme determination for prestressed force (Shenoy & Frantz, 1991).

Two specimens from a 40-year-old inverted T-beam prestressed concrete bridge were tested after deconstruction (Halsey & Miller, 1996). For the prestress loss

determination, they used three methods, one of them being the cracking method. They made some assumptions: (1) All dead load was carried only by the inverted T-beams; these assumptions are valid because the beam weight and the concrete fill were the only dead load. The complete composite section resisted the applied load. (2) The top and bottom strands will not have the same loss. For computation simplification purposes, all strands were assumed to have the same effective prestressing force, so this calculation resulted in an "average" loss per strand. Moreover, they highlight that the main problem with using it is that it has a high dependency on the module of rupture. Code equations for modulus of rupture are approximate at best, and there may be a significant variation of the measured value of such modulus for concretes with similar strengths.

Decompression load

The decompression load method is a widely accepted destructive determination approach for residual prestress force in a concrete member. It has been previously applied in numerous evaluations of full-scale members by various authors, e.g. (Bagge et al., 2017; Labia et al., 1997).

However, in most studies, beams were removed from the site for laboratory testing under simply supported conditions. Bagge et al. (2017) performed this type of test on a bridge still in its service location.

This method is considered destructive as it requires the member to be pre-cracked. It consists of calculating the prestress force corresponding to the load required to reopen an existing crack; at the immediate crack reopening, there is implicitly zero stress in the concrete. To perform it, a specific crack must be monitored at the surface (by recording strains just beside it or displacements across it). At the same time, the member is subjected to an external load aiming to generate the reopening of the crack. The measured response can be either strain or displacement of the crack, and

it showcases a linear variation in relation to the load up to the so-called decompression load; beyond this level, the crack reopens, and a dramatic change in stiffness occurs (Bagge et al., 2017).
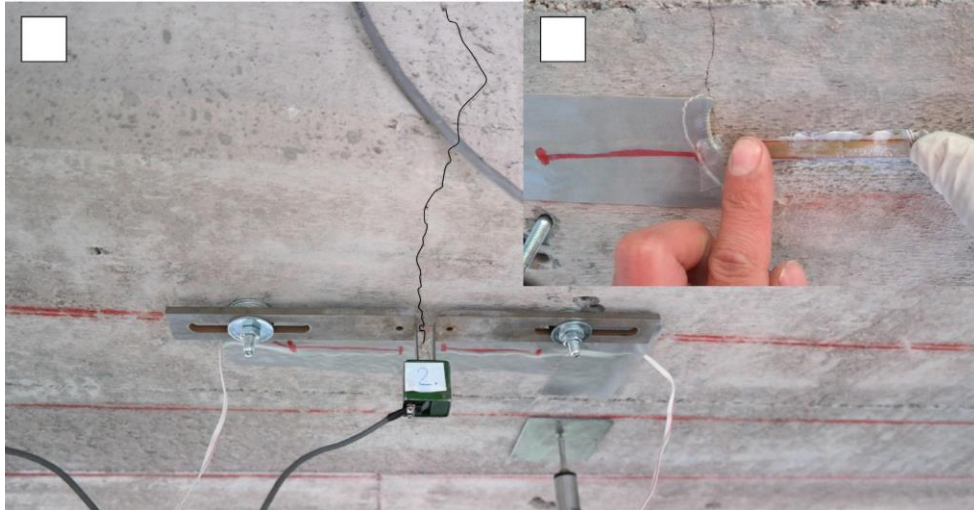
Figure 12. Crack decompression monitoring (Bagge et al., 2017).

Navier's formula can determine the prestress in combination with the decompression load and the effects induced by the other loads acting on the structure. According to:

$$\sigma = \frac{P}{A} + \frac{(P \cdot e_y)\, y}{I} + \frac{M_G y}{I} + \frac{M_Q y}{I}$$

Where:

σ: longitudinal concrete stress at the surface, assumed to be zero.

P: prestress force,

A: cross-section area,

e_p: eccentricity of the prestress force,

y: distance to the neutral axis from the monitored surface,

I: second moment of inertia of the cross-section,

M_G: moment due to dead load,

M_Q: moment due to external loads (in the evaluated section of the member in an uncracked state).
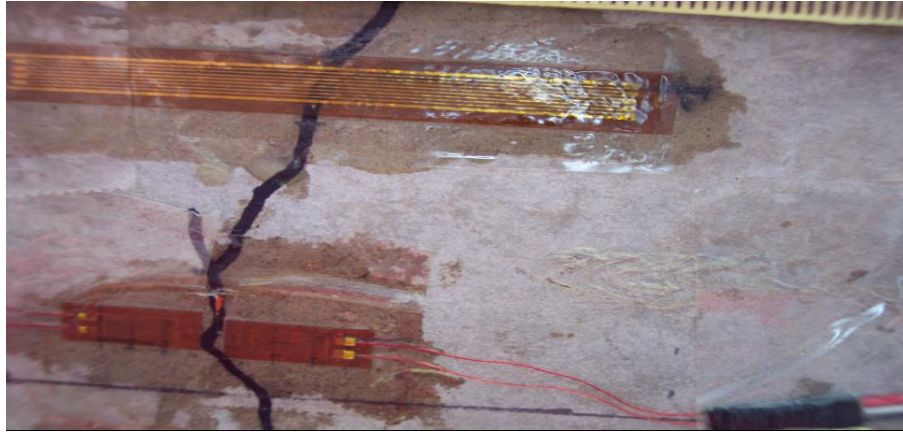
Figure 13. Strain gauges to identify crack reopening (B. M. Kukay, 2008).

Strand cutting

In a strand-cutting test, a strand is exposed, then a strain gauge is installed and used to measure the strains that develop when the strand is cut. The corresponding prestress force in the strand can then be determined (Bagge et al., 2017). The strand-cutting method should be independent of the concrete's internal state of stress, for this reason, it should be an accurate method for computing the current prestress (Labia et al., 1997).

The method has been applied by several researchers before. (Halsey & Miller, 1996) exposed a 305 mm section of a strand in the bottom of a PC beam, the strand was cut using bolt cutters after instrumenting a single wire of the strand with a strain gauge, the authors affirm that this method gives much higher loss than other methods used on the same study as a local loss of prestressing force may be generated when removing the concrete and exposing the strand. In another study, (Baran et al., 2015) used two beams used previously on load tests and exposed

approximately 508 mm of two strands on each of the beams, they instrumented with strand gauges three wires on each strand, and flame-cut them; they conclude that this method is one of the most "effective ways of determining prestress losses in prestressed concrete beams" along with using vibrating wire gauges embedded in the concrete. It was also applied by (Labia et al., 1997) on box girders, where nine strain gauges were mounted on three strands.
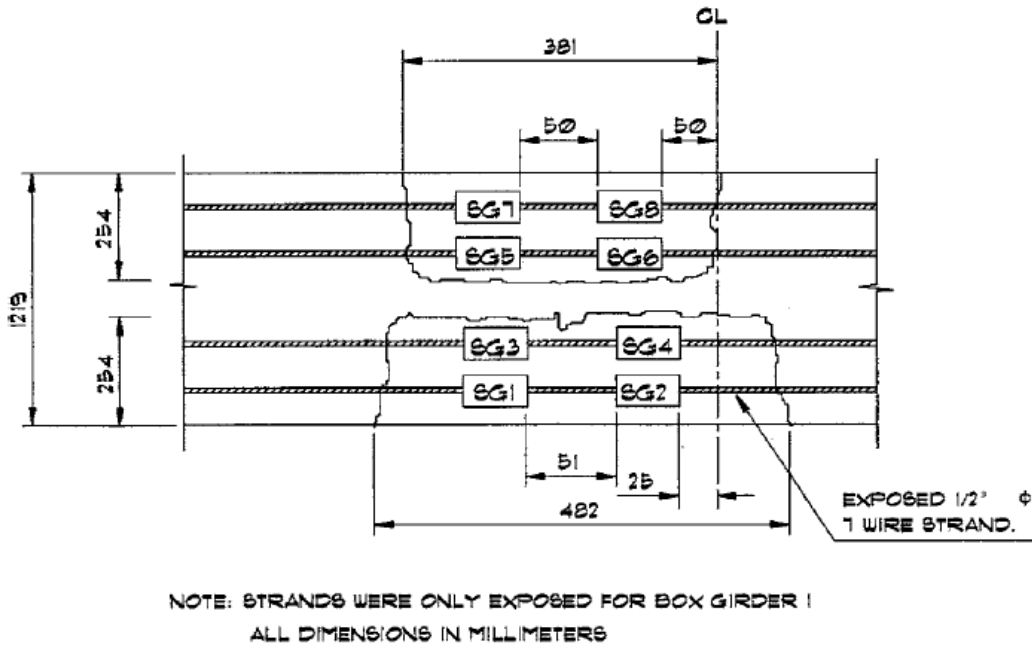
Figure 14. Strand cutting scheme on (Labia et al., 1997).

3.2. Non-destructive methods

Exposed strand

The residual prestress forces can be derived for exposed strands by comparing responses to lateral forces applied to the strands with calibration data (Bagge et al., 2017). In 1998 (Civjan et al.) developed a prototype instrument that can be used to estimate the stress level in exposed prestressed strands in existing members. The stress level is determined by the lateral force applied to an exposed strand and by

measuring the resulting displacement.

In (Civjan et al., 1998) work, their prototype is described as "a simple, compact, and inexpensive tool designed to determine the prestress force remaining in an exposed strand", the instrument works by applying a series of incremental loads perpendicular to a strand while the lateral strand displacements. A calibration graph is then used to compare the load-displacement graph slope, from which the stress on the strand is determined.

The device developed by (Civjan et al., 1998) consists of a frame containing roller-bearing pegs that rest against the strand. Load is applied through a high-strength grasping peg aligned with a load cell. A nut is tightened along a threaded rod for the load application, and a dial gauge attached to the frame record the measured displacements. The final prototype requires only an external voltage source and a voltmeter, being well suited to be used in the field for existing bridge girders. The authors also looked for the instrument to have minimized dimensions to ensure its placing between strands in case of closely spaced multiple-strand arrangements typical in prestressed concrete I-shaped girders.
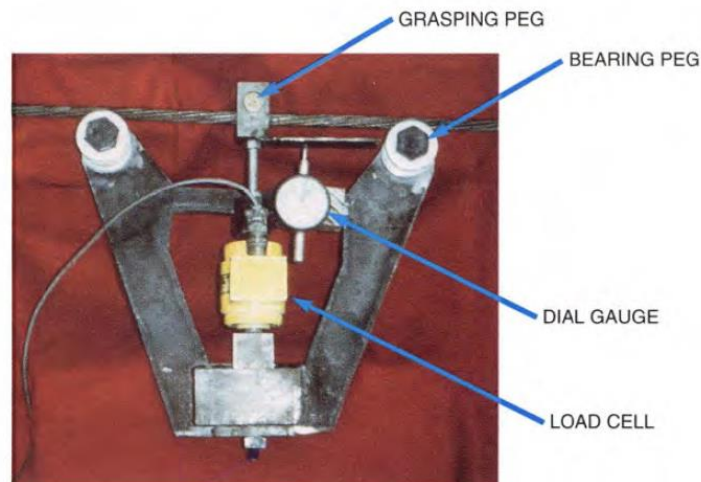
Figure 15. (Civjan et al., 1998) *Prototype plan view*.

In the same article, (Civjan et al., 1998) mention that they found two devices using a similar principle:

(a) A commercially available device that requires a minimum of 850 mm (33.4 in) of exposed wire length and can be used up to 13 mm (0.5 in) diameter strands, and

(b) The California Department of Transportation developed a comparable instrument in 1968.

Both devices are developed for measuring stresses in strands in a prestressing bed or guy wire, while they are not concerned with the constraints of multiple closely spaced strands and short exposed strands length as found in damaged girders. In this aspect, the (Civjan et al., 1998) instrument has an advantage due to its compact size.

Figure 16. (Civjan et al., 1998) *Prototype during splice test.*

Drilled hole

For embedded strands, measurements of stresses around a drilled hole (Fig. 1e) adjacent to the prestressed reinforcement can be used to quantify the residual prestress forces (Bagge et al., 2017). This method has only been applied and confirmed for relatively simple members (in terms of support conditions, member geometry, and prestressed reinforcements) in controlled environments, which means this non-destructive method has never been applied to continuous members reinforced with parabolic post-tensioned cables. (Bagge et al., 2017).

(Azizinamini et al., 1996) Describes this method as an investigation "of the state of stress around a hole in a prestressed concrete member." The procedure is as follows, on the bottom flange of a prestressed girder, a cylindrical hole is drilled (the bottom flange is assumed to be under compression, the following descriptive figure is to be found in the same article
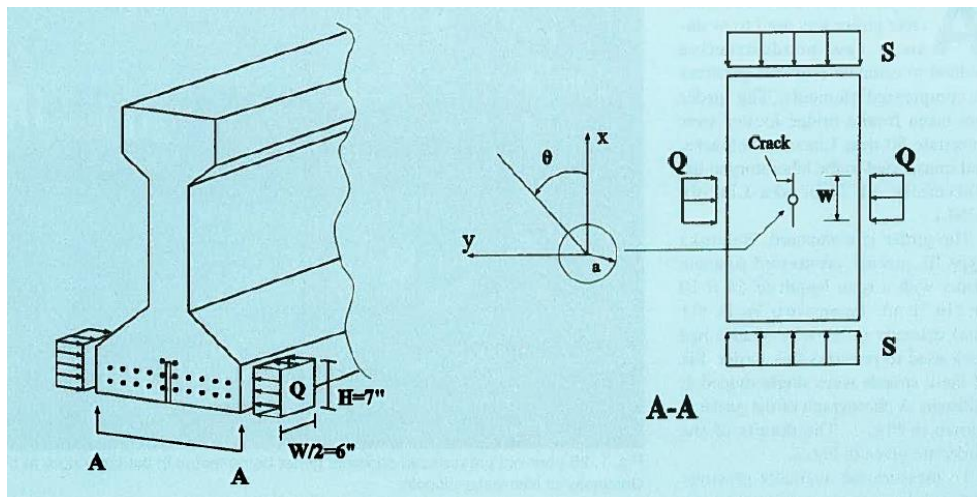
Figure 17. Sectional view of a drilled hole test (Azizinamini et al., 1996).

The stress, *S*, can be viewed as the available stress in the bottom flange of the prestressed girder, *Q*, is the side pressure, this is a known applied pressure over a width *W*, and a depth *H*. (Azizinamini et al., 1996) stands that the hoop stress, $t_{\theta\theta}$,

can be expressed using the following expression.

$$\beta S = \gamma Q - t_{\theta\theta}$$

Where:

β: Stress concentration factor associated with the available stress along the flange at the specified coordinate.

γ: Concentration factor associated with the side applied pressure.

S: Axial stress.

The main objective is to determine the axial stress S, which requires the knowledge of β, γ, and $t_{\theta\theta}$. Determining the value of hoop stress for an arbitrary value of side pressure Q at a specific location in concrete is a difficult task. So, in order to simplify the approach, the objective is to seek a corresponding case of zero hoop stresses ($t_{\theta\theta} = 0$). Such stress state is accomplished by pre-cracking a drilled hole in the bottom flange to ensure that the crack runs parallel to the girder span and detects the span's closing after applying a side pressure, Q.

An indicator that the stress normal to the crack surface at the hole perimeter is the immediate moment when complete closure is achieved at the crack, in such case, the previous equation becomes:

$$S = \frac{\gamma Q}{B} = KQ$$

Where K is the ratio of the available stress, S, to the side pressure, Q, at complete crack closure, this factor can be computed by numerical investigation.

This technique proposed by (Azizinamini et al., 1996) is summarized in the following steps:

1. Drilling of a hole in the bottom flange of a PC element.
2. Pre-cracking the hole to ensure the crack initiation at coordinates $(a, 0°, 0)$ and run parallel to the girder span. This crack should be small, approximately 25 mm in diameter.
3. Increasing the side pressure, Q, over a limited width, W.
4. Determining the side pressure, Q, at which the crack just completely closes.
5. Using the side pressure, Q, corresponding to the crack closure, and an appropriate K factor obtained from the analysis. We can obtain S from the previously showcased equation, that is, the available stress at the extreme fiber of the bottom flange of the prestressed girder.

Performing an experimental study on small block specimens, (Azizinamini et al., 1996) determined that the optimal dimensions for the drilled hole should be 25 mm in diameter and 150 mm in depth; these suggestions are based on practical limitations such as strand spacing in prestressed girders. Although, in field applications, it may be feasible to reduce the depth.

Saw-cuts (Concrete-relax).

In 2010 (Kukay et al.) introduced a new method as an alternative to the traditionally used techniques. This new method consists of saw-cutting small sections on the bottom of the bridge where a strain gauge was placed previously. The objective of the saw-cuts is to isolate the small section of concrete from any stress induced by external loads or prestress. Then the strain change produced from the isolation after the cutting can be correlated to the residual prestress force in the girder's tendons (Bagge et al., 2017; B. Kukay et al., 2010). As in the drilled-hole method, the saw-cuts method has only been applied to relatively simple members in controlled environments (Bagge et al., 2017).
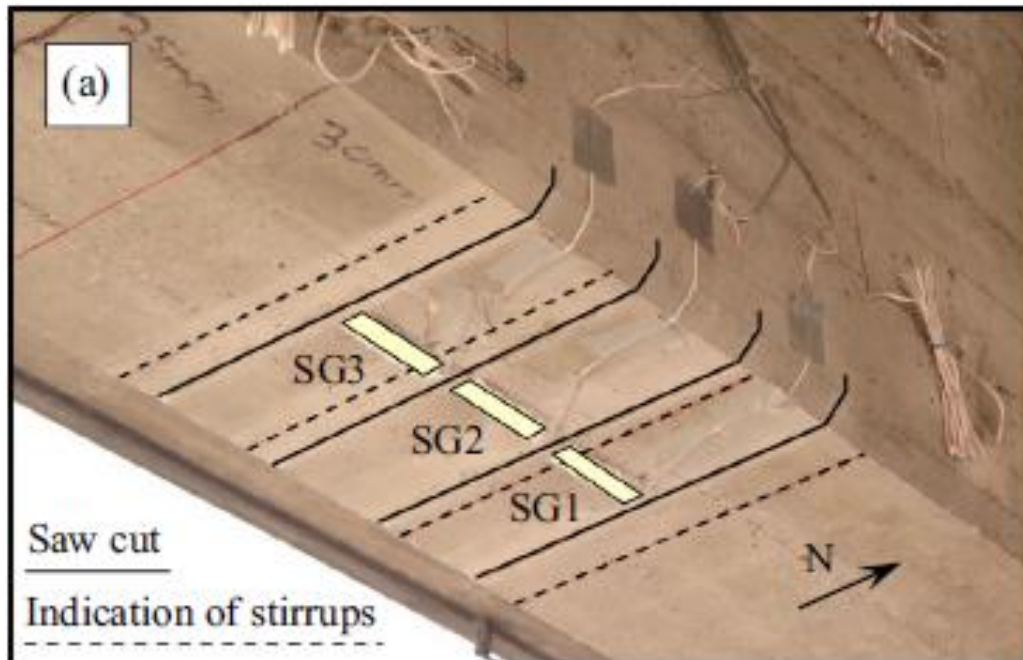
Figure 18. Cuts at the bottom flange of a beam and strain gauges (Bagge et al., 2017).

As previously mentioned, the prestress force can be calculated from the strain corresponding to a fully isolated concrete surface. Isolation is considered complete when increases in saw-cut depths do not lead to further surface strain changes (Bagge et al., 2017).

The following factors must be accounted for as they contribute to the strains at the monitored point (Bagge et al., 2017):

(a) Prestress force in the member, including the influence of eccentricity in prestressing element positions,
(b) restraint forces due, for instance, to eccentricity in prestressing element positions in members that are not free to deform,
(c) the dead load of the member, and
(d) the external applied load.

Considering the factors mentioned above to calculate the residual prestress force, we can use Navier's formula (Bagge et al., 2017; B. M. Kukay, 2008):

$$\sigma = \frac{P}{A} + \frac{(P \cdot e_y)\, y}{I} + \frac{M_R y}{I} + \frac{M_G y}{I} + \frac{M_Q y}{I}$$

Where:

σ: longitudinal concrete stress at the surface,

P: prestress force,

A: cross-section area,

e_p: eccentricity of the prestress force,

y: distance to the neutral axis from the monitored surface,

I: second moment of inertia of the cross-section,

M_R: secondary moment due to restrain forces,

M_G: moment due to dead load,

M_Q: moment due to external loads (in the evaluated section of the member in uncracked state).

Then, using Hooke's law, the measured and calculated strains can be compared, and the prestress force can be determined using an iterative process.

The saw-cuts non-destructive method is only suitable to be applied in situations where the possibility of completely isolating a concrete block from the prestress forces exists. In existing structures, this is not always possible because, in some cases, it is possible to damage non-prestressed reinforcement as it may be located too close to the concrete surface to make sufficiently deep saw-cuts. For those situations (Bagge et al., 2017) suggest that complementing the saw-cuts method with a FE analysis may provide valuable complementary information.
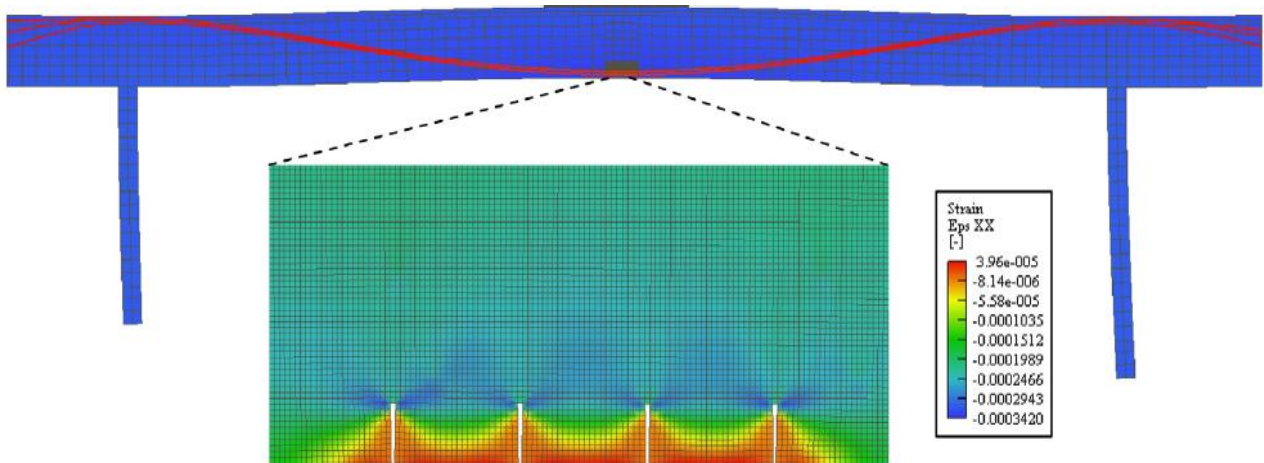
Figure 19. FE model for non-destructive evaluation used by (Bagge et al., 2017).

4. Experimental campaign.

BRIDGE|50 is a wide experimental campaign where several prestressed concrete members 50-year-old dismantled from the Corso Grosseto bridge are subjected to destructive and non-destructive testing to obtain data that can be used to assess the structural behavior of existing structures at the end of their service life. This data can give a statistical description of degrading phenomena and corresponding structural behavior of bridge beams, improving the safety, maintenance, and management of existing infrastructure systems (Biondini, Tondolo, et al., 2021; Tondolo et al., 2021). The planned research activities on the project include photographic mapping, drone surveys, corrosion measures, non-destructive testing (ultrasonic test, rebound hammer test, SONREB method), full-scale tests, and several laboratory tests on a large number of samples extracted from the tested elements(Anghileri, Biondini, et al., 2021; Anghileri, Savino, et al., 2021; Tondolo et al., 2021). The performed tests for this thesis are included in the scope of the BRIDGE|50 research project.

4.1. Bridge and beams description.

The studied beam elements belonged to the Corso Grosseto viaduct in Turin, Italy, a road bridge built in 1970 as a response to the uprising traffic and urbanistic problems generated by the fast development of the industry in the city and the vast increment of citizens. The bridge consisted of a simply supported girder system with precast prestressed beams and cast in-situ concrete slab, which was subjected over the years to several deterioration causes mainly generated by exposure to aggressive agents. The bridge closure and deconstruction were performed between 2018 and 2019.

The technical aspects of the viaduct are presented by (Savino et al., 2021). The viaduct was composed of a total of 80 simply supported spans with their lengths varying from 16 m to 30 m., the deck girder was composed of ten precast PC I-shaped beams and two box beams at the edges, generating a total of 8 m. Over the beams, there was a 14 cm concrete slab cast in situ; also, to complete the deck, there were two intermediate cast-in-place concrete transverse beams. The maximum height reached from the ground was 12.43 m. Details of the viaduct during its construction phases and completion are presented in figure 8.

In the original documents, the first solution to be found in the documentation is a prestressing system of post-tensioned wires with curved profiles along the beam, as mentioned in (Savino et al., 2021). The authors also speculate that this solution was modified by the general contractor for a faster and more economical straight-strand solution.
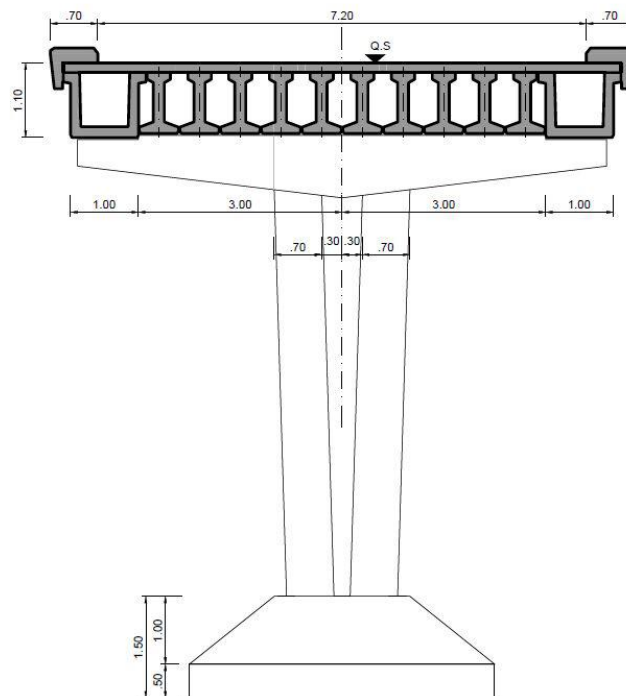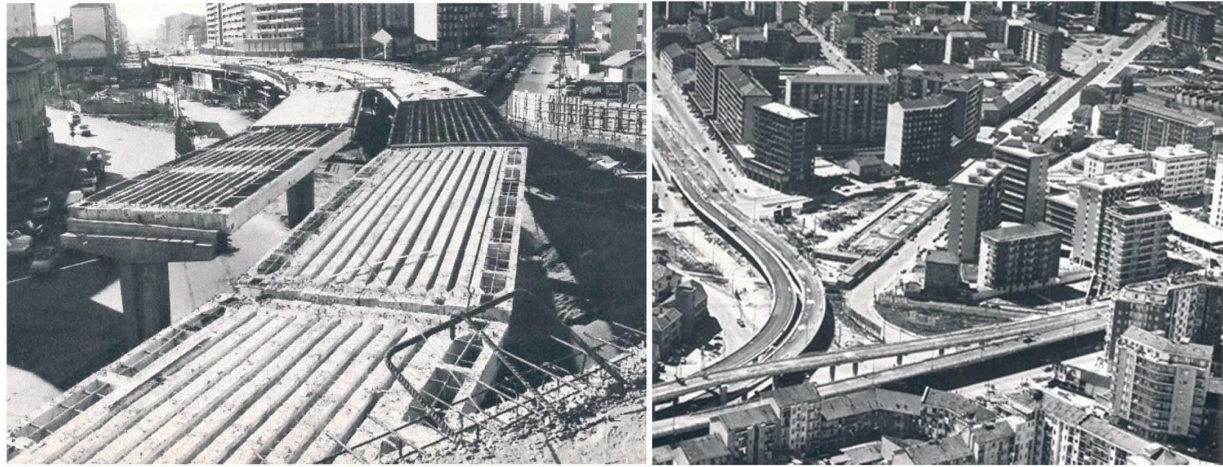
Figure 20. (a) Detail of the viaduct during the construction phases. (b) Corso Grosseto Viaduct, Torino (Italy), year 1970 (Impresa Pessina 1976) (Savino et al., 2021). *(c) Bridge deck cross-section* (Biondini, Tondolo, et al., 2021)

The prestress strand reinforcement is as follows:

- For double I-beams: 20 straight 1/2" diameter strands.
- For box beams: 40 straight 1/2" diameter strands.

For both beam typologies, the characteristic ultimate stress is about 1640 MPa. The prestressing reinforcements were not bounded for the entire length of the elements;

51

they were unbonded on the end sections and bonded in the transition area. Four strands were unbonded for the I-beams, and 11 strands were unbonded for the box beams. The prestressing action was extensively used to speed up the construction process. Figure 9 shows the beam typologies.
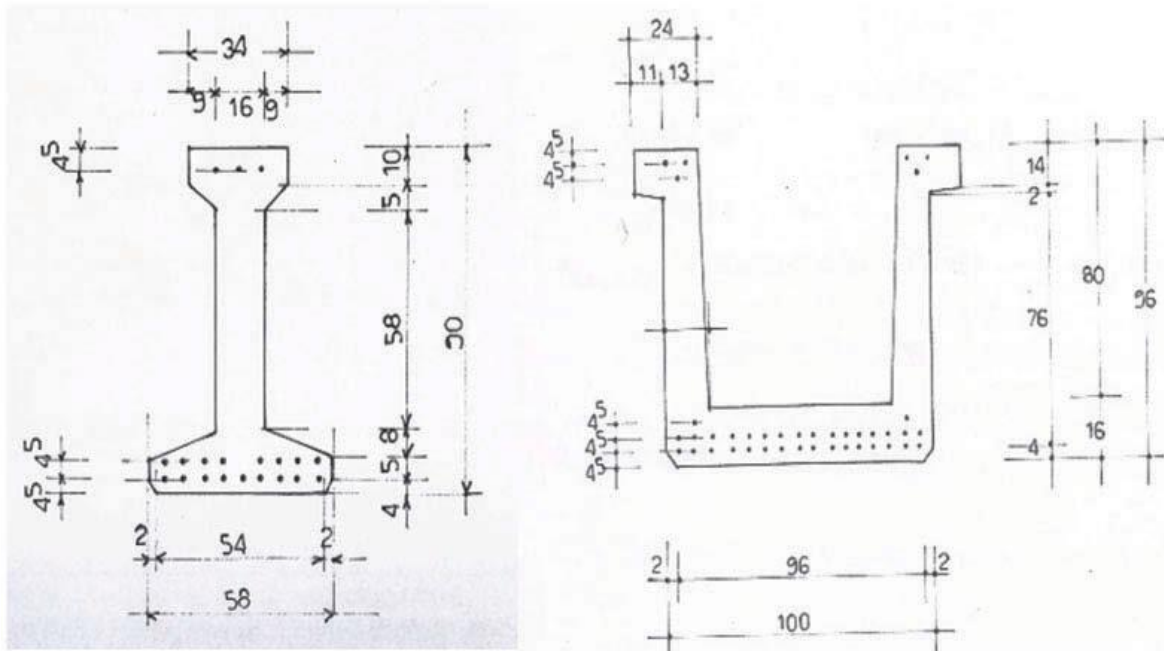
Figure 21. Double T-beam and U-beam cross section typologies (Savino et al., 2021)

The piers consisted of an inverted T shape where the cap of the pier, that is, the transverse of the T-shape, was post-tensioned through prestressing tendons with multiple smooth wires. Such caps were made of cast in-situ prestressed reinforced concrete using a post-tensioned prestressing system with 36, 24, and 18 smooth wires along a curved profile with a diameter of 7 mm and ultimate characteristic resistance of about 1620 MPa. The concrete was designed for a minimum characteristic cubic resistance of 30 MPa at 30 days (Savino et al., 2021). Two different phases were performed for the members' total prestressing: a prior prestressing transferred before the placing of the beams and a secondary prestressing applied before the introduction of non-structural loads.

Two cast in-situ transverse beams are placed at 1/3 of the span, allowing a girder

behavior by connecting the longitudinal beams. These transverse beams improve the torsional behavior of the longitudinal beams and the restrain degree working along with the slab. The slab works as a load distributor to the beams, determining, along with the transverse beams, the entire combined resistance effect of the deck.

The tests described in this work are performed in double-T-type beams, which are presented in detail in the following figure.
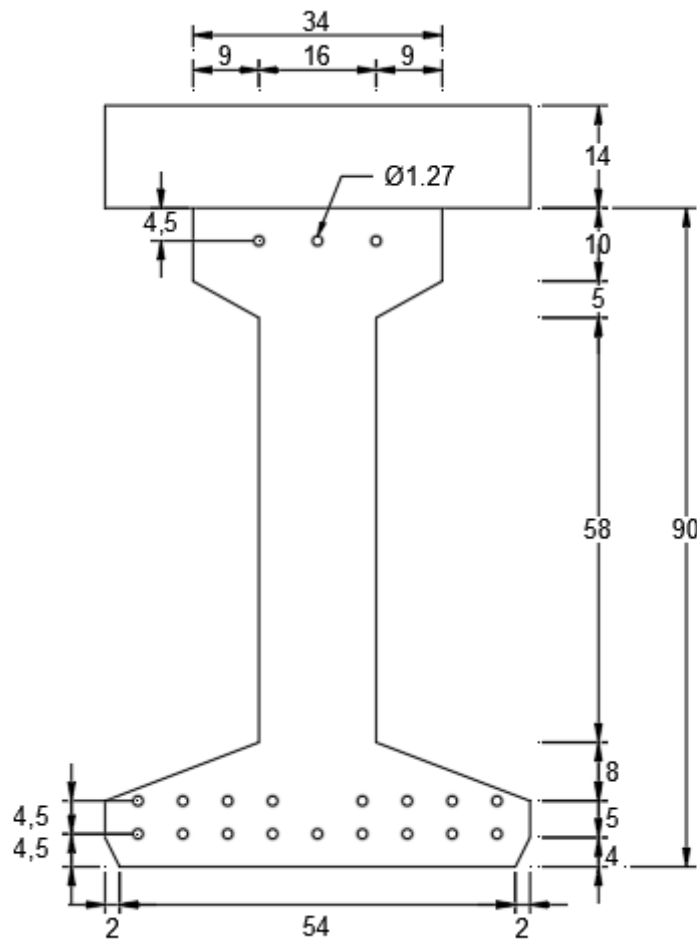
Figure 22. Detailed geometry of double- T beams.

The top flange of the beam is 34 cm in, and 10 cm in height with a 5 cm high chamfer until the total width reaches 16 cm in width. The web is 16 cm wide by 58 cm high. The bottom flange is 58 cm wide and 9 cm high with a top chamfer of 8 cm and a

bottom smaller chamfer of 2 cm on each side. There are 20 prestress strands with a diameter of 1/2" (1.27 cm), 3 in the top flange and 17 in the bottom flange.

On the original designs of the bridge (Ufficio Tecnico Lavori Publici - Città Di Torino, 1970) the characteristic tensile stress of rupture is $167 \ kg/mm^2$, the tensile stress correspondent to the 1% of the deformation is:

$$R_{ak} = 0.9 * 167 = 150.30 \frac{kg}{mm^2}$$

The admissible prestress in the moment of precompression of the beam element is:

$$\sigma_{api} = 0.95 * 150.30 = 142.79 \frac{kg}{mm^2} = 1400.77 \ MPa$$

The strand prestress losses are:
- Shrinkage: $6.00 \ kg/mm^2$
- Creep: $18.65 \ kg/mm^2$
- Elastic shortening: $8.11 \ kg/mm^2$
- Steel relaxing: $24.78 \ kg/mm^2$

The computed theoretical total prestress losses are:

$$6.00 + 18.65 + 8.11 + 24.78 = 57.54 \frac{kg}{mm^2} = 564.47 \ MPa.$$

So, the theoretical total remaining prestress level on the strands is:

$$\sigma_{ap} = 142.79 - 57.54 = 85.25 \frac{kg}{mm^2} = 836.30 \ MPa$$

Testing site.

The beams are stored in an open space at the Politecnico di Torino campus at Mirafiori, south of Torino. In the place are stored 29 prestressed concrete (PC) deck beams, of which 25 are I-shaped beams, 4 are box beams, and 2 pier caps.

Figure 23. PC beams at the working site.

As part of the BEAM|50 project, all beams are load-tested up to failure. For this purpose, it was specifically designed a reaction steel frame, such loading frame configuration can be modified to perform either a three-point bending test or a four-

point bending test. Some beams are loaded in a specific way looking for pure flexural failure, and some are loaded looking to see the interaction between flexural and shear failure; the beams have a specific code in order to identify them, and the order of the loading tests is previously determined. The special loading frame is presented in figure 24.

Figure 24. PC beam on loading frame.

4.2. Experimental tests.

Concrete relax test.

The concrete relax tests measure the strains on a small concrete block detached from the bottom flange of the prestressed members. When the small block is completely isolated from the rest of the concrete member, the compression strains caused by the prestressing strands stresses do not affect it anymore, so measuring how much the

microstrains at the concrete change while it is being separated from the member it is possible to compute how much are the prestress levels inside the member.

The used strain gauges are 20 mm long, and the cuts are performed 15 mm from each end of the gauge to avoid affecting the cable connections attached to one of the gauge's ends. An electric rotatory saw is used to perform the cutting. Initially, the cuts were meant to be perpendicular to the beam's longitudinal axis, as shown in the following image.

Figure 25. Concrete relax test on beam 1, point A (left), and point B (right).

However, this methodology of cutting involved four cuts to completely detach the small block: two lateral cuts, one on top, and one at the bottom; which made it too complicated to reproduce and prone to errors; At the same time, the bottom cut involved an elevated risk for the operator of the saw which should place himself in an uncomfortable position to perform it. It was then decided to perform two cuts, starting at the same position, 7 cm from each other, but inclined 45° with respect to the vertical plane of the beam's longitudinal axis, meeting at the prolongation of the center of the strain gauges a generating a prism with an isosceles triangle on the to face.
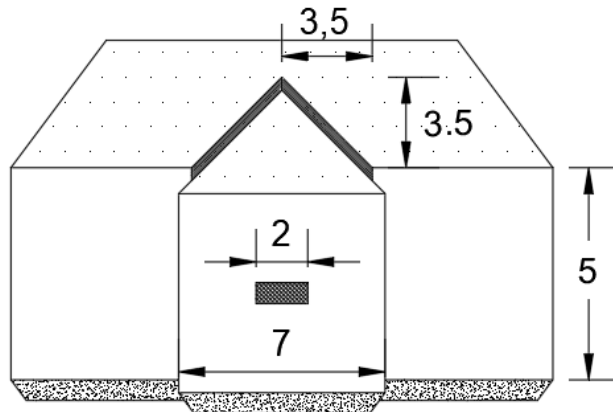
Figure 26. Concrete relax test geometry in cm.

The figure shows the geometrical scheme for the test. Figures present the progression in the test cuts.

Figure 27. Concrete relax test. Before (a), mid (b) & after (c).

Knowing the strain is possible to use Hook's law and Navier's equation for stress in a bending beam to obtain the prestressing stress in the beam.

$$-\varepsilon_c * E_c = \frac{M_q}{I_{om}}(Y_G - C_z) - \frac{P * e}{I_{om}}(Y_G - C_z) - \frac{P}{A_{om}}$$

Where:

σ_p: Residual prestressing stress.

ε_c: Measured strains in the concrete.

E_c: Young modulus for the concrete.

P: Total prestressing force.

M_q: Bending moment due to dead load.

I_{om}: Second moment of area or second moment of inertia.

Y_G: Center of mass coordinate.

C_z: Strain gauge coordinate.

e: Excentricity.

A_{om}: Cross-section area.
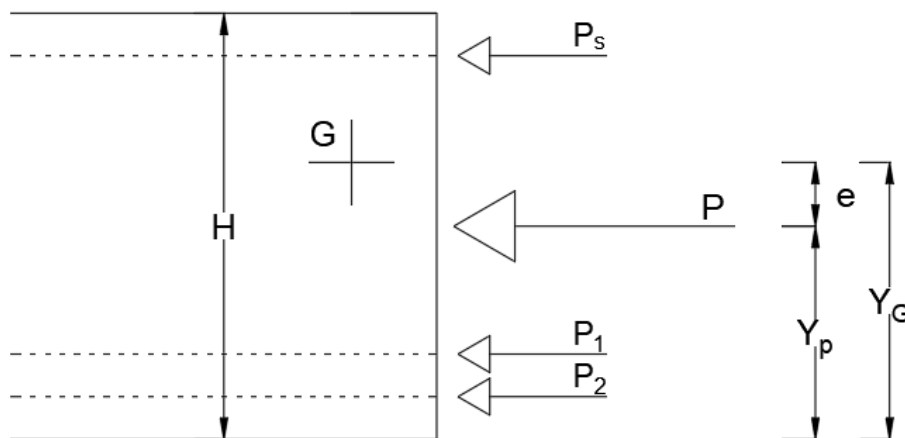
Figure 28. Force scheme of the section.

In this equation, the value of the total prestressing force (P) is the sum of each of the resultants for each prestressed strand level:

$$P = P_s + P_1 + P_2 = \sigma_s * A_s + \sigma_1 * A_1 + \sigma_2 * A_2$$

For simplicity, we assume that the stress on each strand row is equal $\sigma_s = \sigma_1 = \sigma_2 = \sigma_p$. We have then a three unknown system and just two equations. The third equation is obtained from the rotation equilibrium of the section:

$$P * Y_p = P_s * Y_s + P_1 * Y_1 + P_2 * Y_2$$

Solving the 3x3 system and obtaining the stress on each strand row, we can subtract the quantity of these stresses that are caused by dead weight at each level to compute the real remaining prestress levels finally

$$\sigma_{ps} = \sigma_p - \alpha * \frac{M_q}{I_{om}} (Y_G - H + c)$$

$$\sigma_{p1} = \sigma_p - \alpha * \frac{M_q}{I_{om}} (Y_G - 2 * c)$$

$$\sigma_{p2} = \sigma_p - \alpha * \frac{M_q}{I_{om}} (Y_G - c)$$

Steel strand cutting test.

This test measures the strains in compression suffered by a prestressed strand cut. The first two prestressed strands in the bottom flange of the element are exposed by removing its concrete cover using and hydraulic hammer. After the strands are

completely uncovered, a strain gauge is stuck on them; then, the strand is entirely cut along its diameter.

In the first attempts, only a section of the strand was exposed, and the cut was performed just some cm away from the stuck strain gauge. At the moment of each prestressed strand fiber complete cut, it suffered a strong recoil, causing the small welding in the strain gage cables to unstick, so for the first beam's attempts, the measurements were unsatisfactory.

Figure 29. Strain gauge on the steel strand.

Figure 30. First test scheme (cut in red).

As a solution to the problem, two different segments of prestressed strands are exposed; a first segment where the strain gauge is placed and a second segment where the steel is cut. A concrete portion is left covering the strands between the exposed sections, acting as shock absorbers for the recoil impact. When the strand is cut, the left concrete portion is demolished, and with it, the strand portion is entirely free, allowing the strain measurement without the strain gauge being damaged. Figures 28 illustrates the test.

Figure 31. Configuration before strand cutting.

Figure 32. Completely cut strands.

Once the strain on each strand is known, is possible to obtain the corresponding stress on the strand from the measured strain as:

$$\sigma_{st} = \varepsilon_{st} * E_p$$

Where:

ε_{st}: Measured strain.

E_p: Young modulus for the steel.

To this stress, it must be subtracted the stress caused by the flexural moment due to the dead load from the beam to obtain the resulting prestress on the strand:

$$\sigma_{ps} = \sigma_{st} - \alpha * \frac{M_q}{I_{om}}(Y)$$

4.3. Testing program.

In this section is going to be described the order and characteristics of the individual tests performed for each beam. It was previously mentioned, the tests are performed on previously load-tested beams, and the order of these loading tests is already determined by the BEAM|50 project. Table 1 shows the beam loading test order and identification codes.

	Beam #	Beam code
Tested beam 1	8	T3-P46/P47
Tested beam 2	15	T8-P46/P47
Tested beam 3	13	T4-P46/P47
Tested beam 4	16	T9-P46/P47
Tested beam 5	19	T7-P46/P47
Tested beam 6	20	T6-SP/P47

Table 1. Order of tests and beam identification codes.

Tested beam #1, code T8-P46/P47.

The tested beam number 1 showed a clear failure zone that divided the beam into two bodies, each of the two bodies stands in two simple supports. The first body has a total length of 10.3 meters and the failure zone is located at 3.49 m from its last support generating a cantilever. The second body is 8.73 meters long with a cantilever of 1.12 m from the failure zone to its nearest support. The total height of the element is 104 cm, 90 cm from the beam, and 14 cm from the top slab. The medium characteristic strength for the concrete (R_{ck}) is 43.8 MPa; all concrete strength values presented here are obtained from preliminary sclerometer (or rebound hammer) tests, more accurate values will be obtained later after compressive tests.
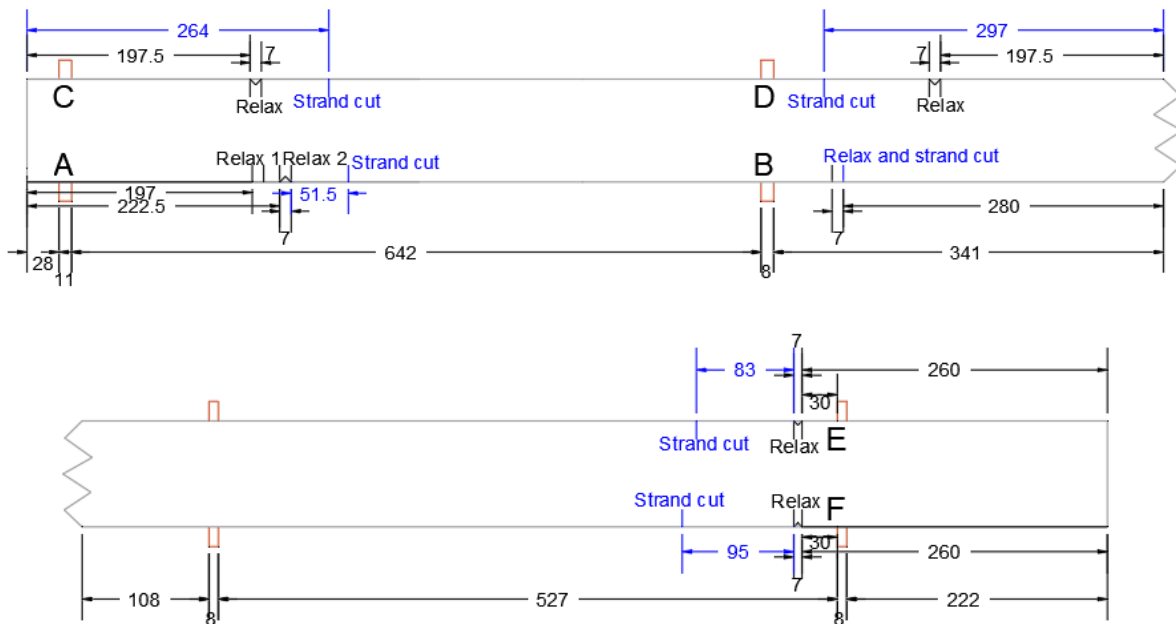
Figure 33. Beam number 1 measures and performed tests location.

This beam has six testing points, four on the first body: A, B, C, and D; and 2 on the second body: E and F. On each testing point were performed a concrete relax test and a strand cut test. On testing point A, two relaxing tests were performed as previously discussed.

Tested beam #2, code T3-P46/P47.

The second tested beam did not show a violent rupture as Beam 1 and its whole body is simply supported with a distance between supports of 17.42 m and a full length of 19.48 m. Each support is located at 0.88 m from the beam ends. The total height of the element is 104 cm, 90 cm from the beam, and 14 cm from the top slab. The medium characteristic strength for the concrete (R_{ck}) is 45.6 MPa.
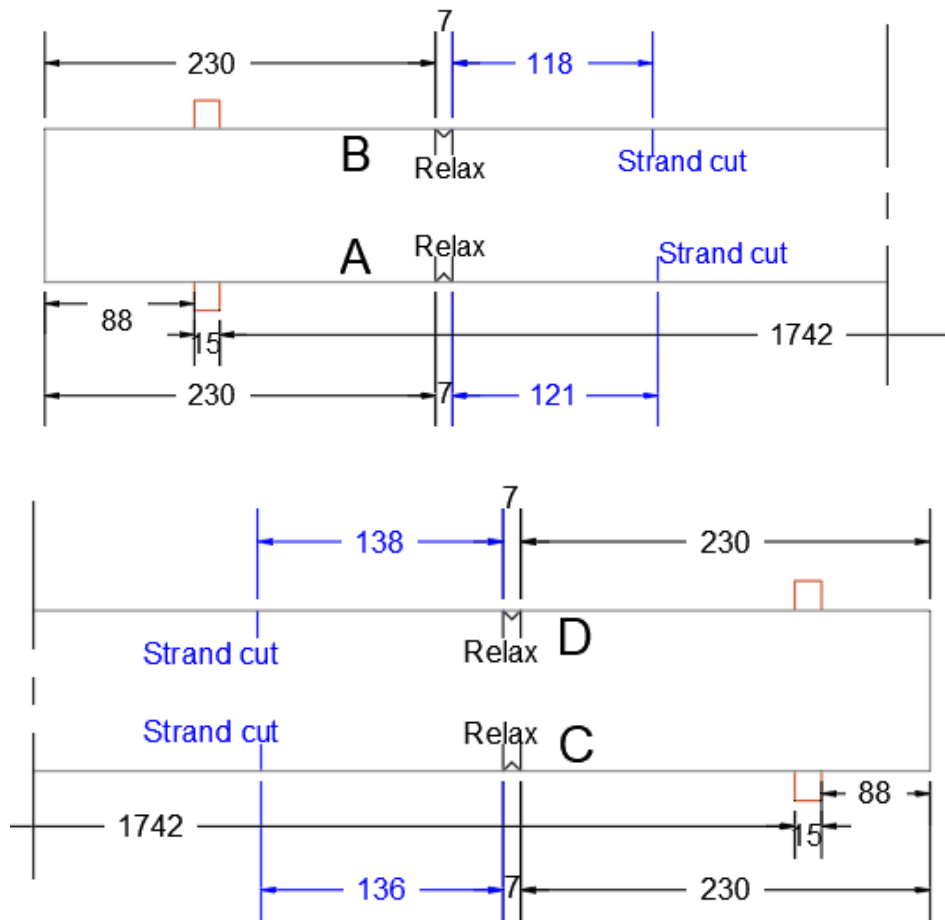
Figure 34. Beam number 2 measures and performed tests location.

For this beam, there are 4 testing points: A, B, C & D; The first two on one end of the beam and the following two on the other end. For each point are performed a concrete relax test and a strand-cutting test. In point B two strands were instrumented and severed.

65

Tested beam #3, code T4-P46/P47.

For beam # 3 once again the element presents a violent rupture and is divided into two bodies, each with a simply supported scheme. The first body has a total length of 8.49 m with a 1.30 m cantilever on the failure part; while the second body is 10.79 m with a 1.38 m cantilever on the failure side. The total height of the element is 104 cm, 90 cm from the beam, and 14 cm from the top slab. The medium characteristic strength for the concrete (R_{ck}) is 39.2 MPa.
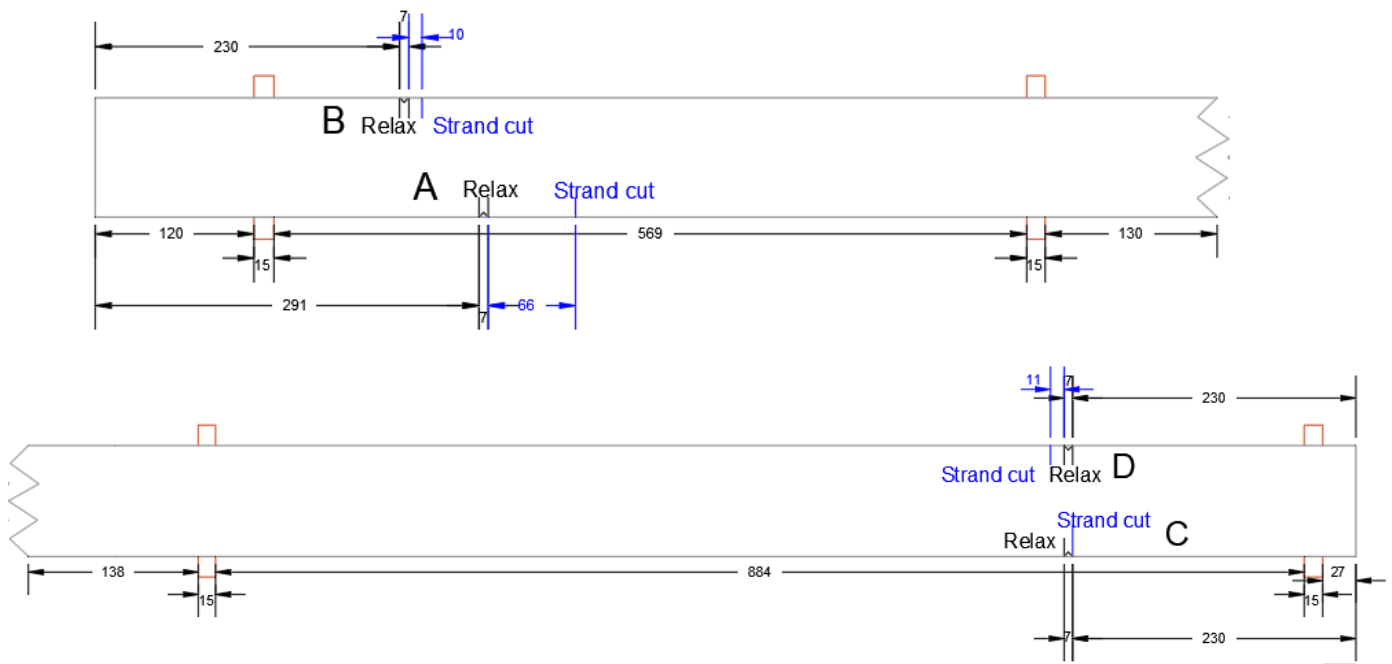
Figure 35. Beam number 3 measures and performed tests location

In this beam there is a total of four testing points: A, B, C & D. Points A and B are located at the end of the first body on opposite sides of the bottom flange of the beam, while points C and D are located in the second body also in opposite sides of the beam. A concrete relaxing test and a strand-cutting test are performed at each one of the testing points. For the strand-cutting test in points C and D, two strands are instrumented with strain gauges for each test.

Tested beam #4, code T9-P46/P47.

Beam #4 shows once again a complete rupture, divided into two bodies simply supported. The first body is 8.36 m long and has a 1.29 m cantilever close to the failure zone; the second body is 10.85 m long and has a 1.11 m cantilever at the failure end. The total height of the element is 90 cm, in this beam there is no slab at the top. The medium characteristic strength for the concrete (R_{ck}) is 43 MPa.
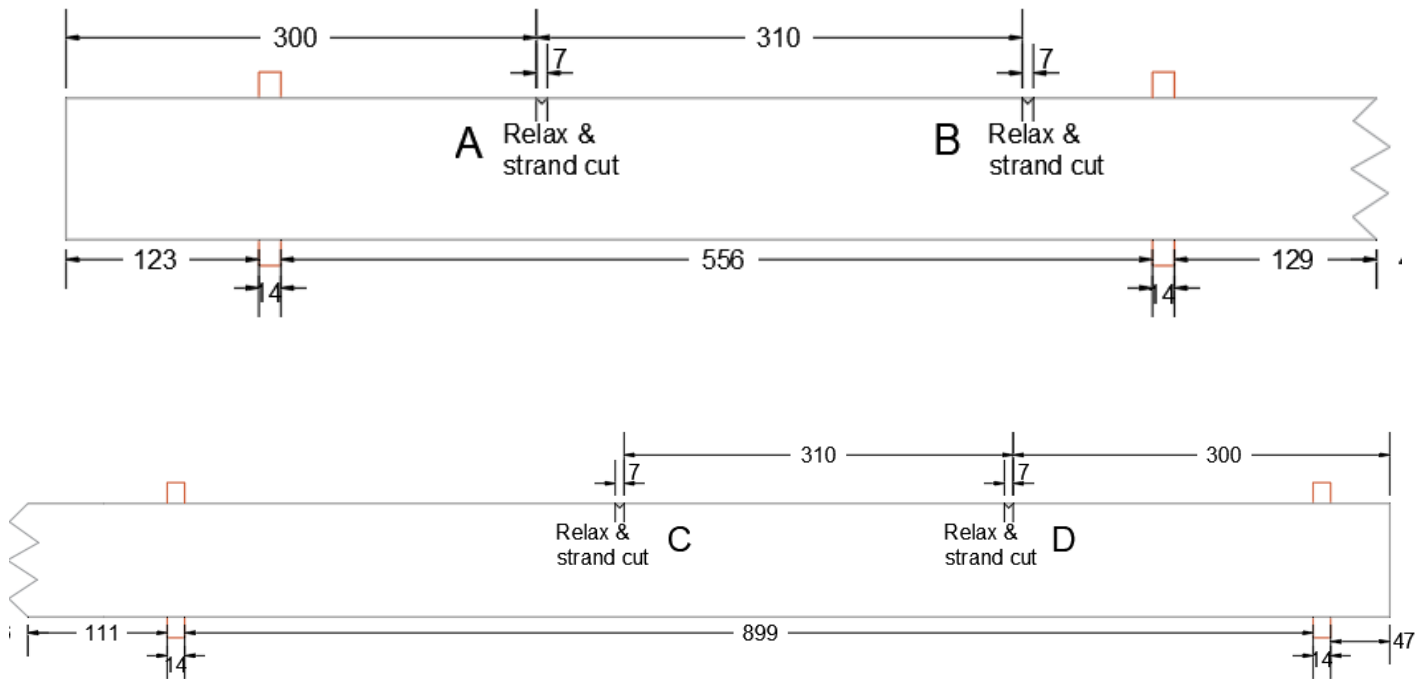
Figure 36. Beam number 4 measures and performed tests location.

Four testing points are defined: A, B, C & D; both, concrete relax test and strand cutting tests are conducted on each point. A and B are located in the first body, and points C and D are located in the other one, in this case, all four points are on the same side of the beam, in the bottom flange. On every strand severing test performed for this beam, two strands are instrumented with strain gauges; for point C, the strands were damaged due to the strands' recoil when cutting them.

Tested beam #5, code T7-P46/P47.

Tested beam #5 failed by compression on the top flange and does not present a full failure zone as beams #3 and #4, the beam is a whole supported body with a total length of 19.55 m, it is simply supported with a central span of 17.66 m. The total height of the element is 104 cm, 90 cm from the beam, and 14 cm from the top slab. The medium characteristic strength for the concrete (R_{ck}) is 50.2 MPa.
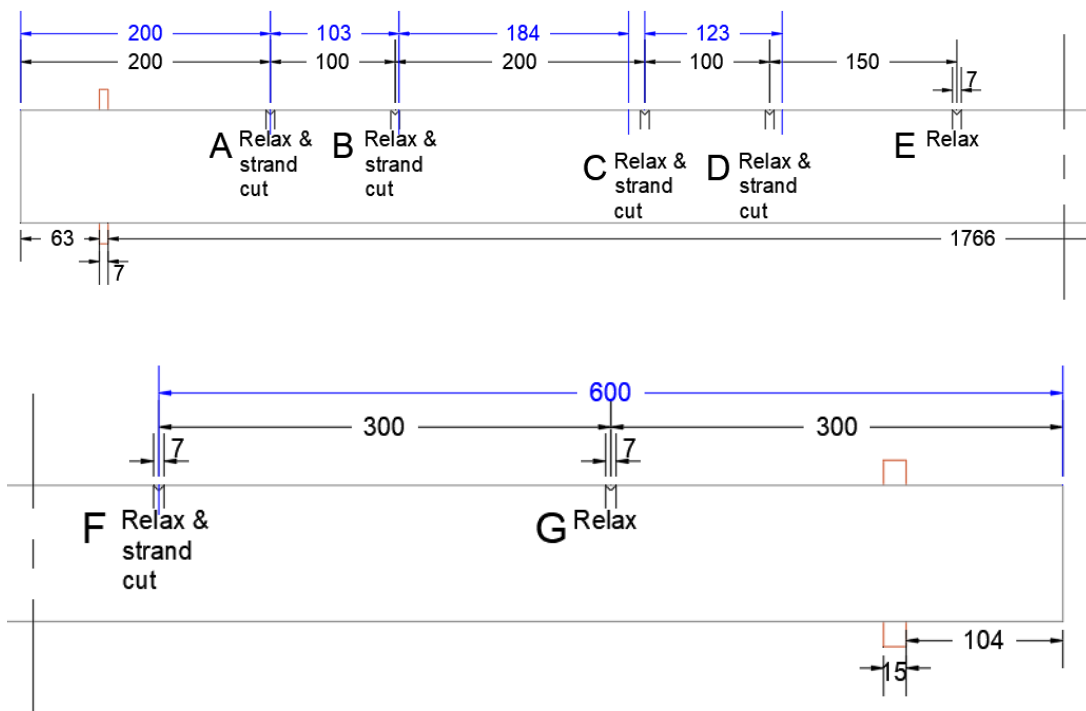
Figure 37. Beam number 5 measures and performed tests location.

Seven testing points are defined for this beam: A, B, C, D, E, F & G. All of them are in the bottom flange, and on the same side of the beam. Five points, A, B, C, D, and E near the first beam end; the remaining two points, F and G located on the other beam end. Concrete relaxing tests are performed on each point while strand cut is performed in points A, B, C, D, and F; for points A and D the strain gauges were damaged during the test.

Tested beam #6, code T6-SP/P47.

Tested beam #6 failed by compression on the top flange as beam #5, the beam is a whole supported body with a total length of 19.55 m, it is simply supported with a central span of 17.36 m. The total height of the element is 104 cm, 90 cm from the beam, and 14 cm from the top slab. The medium characteristic strength for the concrete (R_{ck}) is 45.4 MPa.
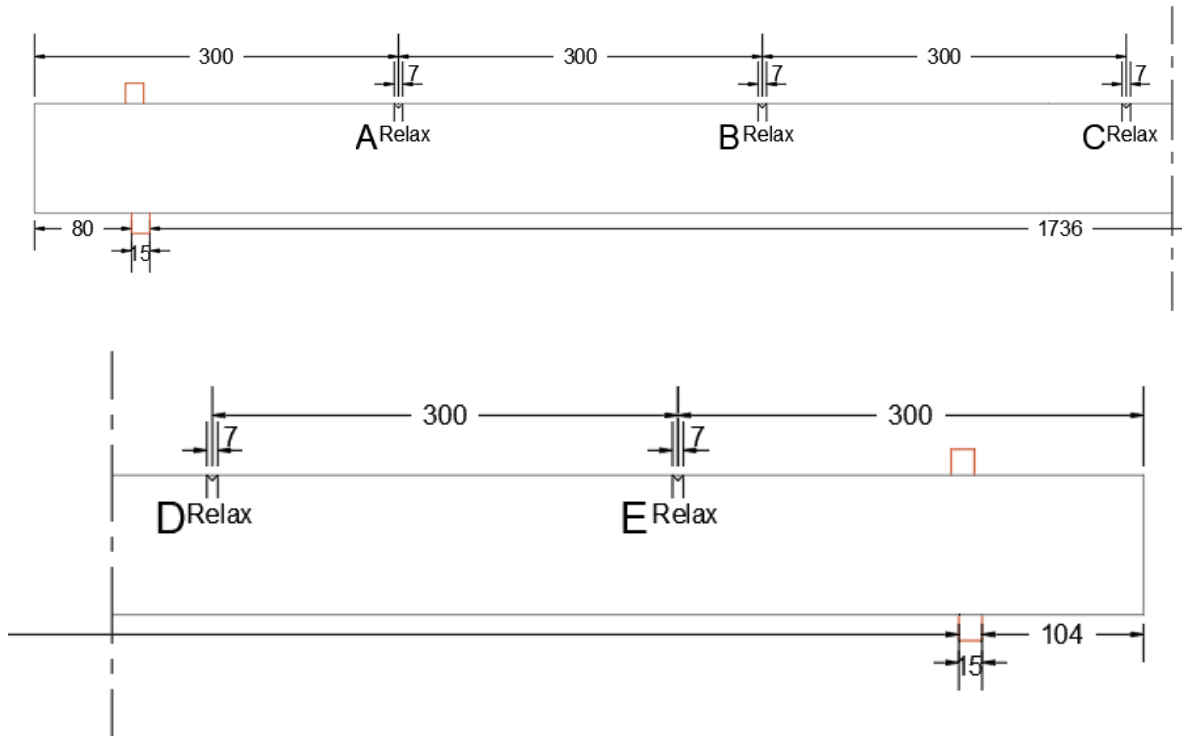
Figure 38. Beam number 6 measures and performed tests location.

Five testing points are defined for this beam: A, B, C, D, & E. All of them are in the bottom flange, and on the same side of the beam. Three points, A, B, and C near the first beam end; the remaining two points, D and E located on the other beam end. Only concrete relaxing tests are performed on each point of this beam.

5. Results and Discussion.

The material properties used for the computations are:

Material Properties					
Test Beam	Ep	Rck	fcm	Ec	Alpha
	[MPa]	[MPa]	[MPa]	[MPa]	
1	190000	43.8	36.354	32403.233	5.864
2	190000	45.6	37.848	32797.109	5.793
3	190000	39.2	32.536	31342.377	6.062
4	190000	43.0	35.690	32224.534	5.896
5	190000	50.2	41.666	33756.485	5.629
6	190000	45.4	37.682	32753.888	5.801

Table 2. Material properties for the beams.

Where:

Ep: Young's modulus for the prestressing steel,

R_{ck}: Concrete cube compressive strength,

f_{cm}: Concrete cylindric compressive strength obtained as $R_{ck} * 0.83$, (E. C., 2005),

E_c: Young's modulus of concrete, computed as $E_c = 22000 * \left(\frac{fcm}{10}\right)^{0.3}$, (E. C., 2005),

α: Transformed section factor Ep/Ec;

The geometric properties of the section computed from the previously presented geometric characteristics of the beam cross-section are:

Geometric properties		
S_{inf}	$[mm^3]$	91289245.8
A_{om}	$[mm^2]$	239324.801
y_G	$[mm]$	381.444988
I_{om}	$[mm^4]$	2.2581E+10

Table 3. Geometric properties for the beams.

The obtained results for the concrete relaxing test are presented in the following sections. The quantity "z" refers to the distance from the middle point of the support

to the location of the strain gauge, and "z_{real}" is the distance from the beam end to the strain gauge location. For the strand-cutting tests, there are several points with missing values, this is due to the damage the strain gauges caused by the strand recoil during the test.

Results beam #1, code T8-P46/P47.

The measured strains in the concrete relax test for beam tested #1 are presented in the following two graphs. The strain gauges used for the steel strands were damaged on the strand cutting so there are no values for such test on this beam.
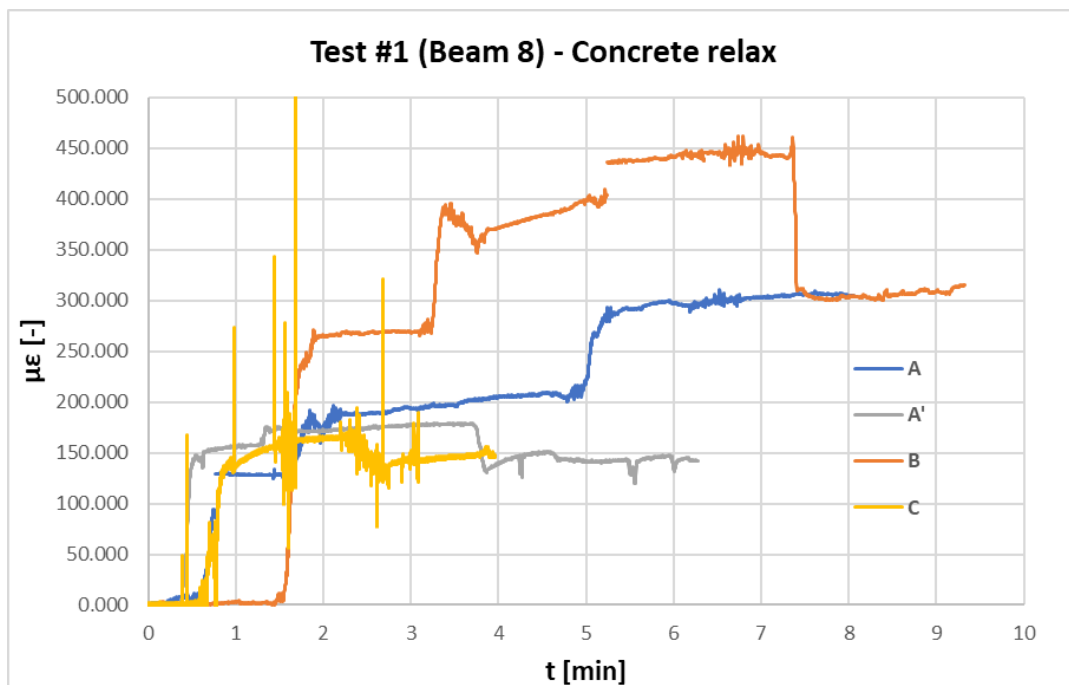
Figure 39. Concrete relax test measured strains on tested beam #1, points A, A', B, and C.
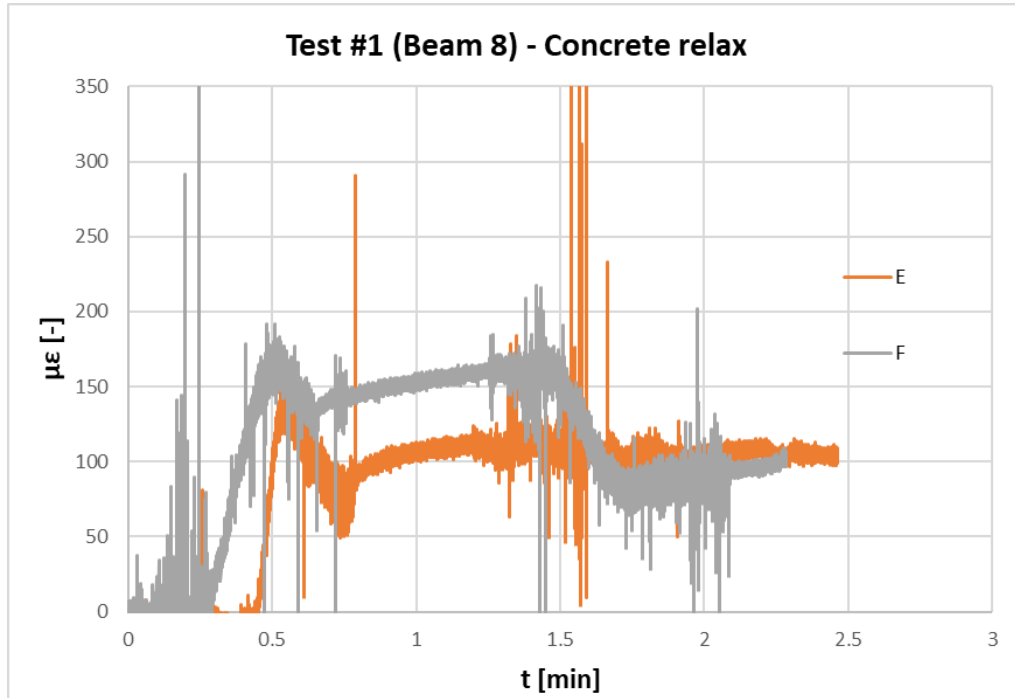
Figure 40. Concrete relax test measured strains on tested beam #1, points E and F.

Beam	Point	Concrete Relax						
		z	z_{real}	Rck_{media}	$\mu\varepsilon$	σ_{ps}	σ_{p1}	σ_{p2}
		[m]	[m]	[N/mm²]	[-]	[N/mm²]	[N/mm²]	[N/mm²]
Test 1 - Beam 8	A	1.670	2.005	43.8	300	1118.930	1116.061	1115.892
Code:	A'	1.925	2.260	43.8	150	573.050	570.017	569.838
T3-P46/P47	B	7.130	7.465	43.8	300	725.944	730.596	730.869
	C	1.675	2.010	43.8	150	571.690	568.817	568.648
	E	4.975	6.095	43.8	100	350.229	351.949	352.050
	F	4.975	6.095	43.8	100	350.229	351.949	352.050

Table 4. Concrete relaxing test results for Beam #1.

Point D results are dismissed as the obtained value is higher than the initial prestressing in the steel strands, probably due to a misreading from the strain gauges. The values for points E and F are also not accurate as they are too low and can be considered dismissed.

Results beam #2, code T3-P46/P47.

On beam #2, data obtained on the concrete relax test was not trustworthy so is not presented. Results for the strand-cutting test on beam #2 are presented below.
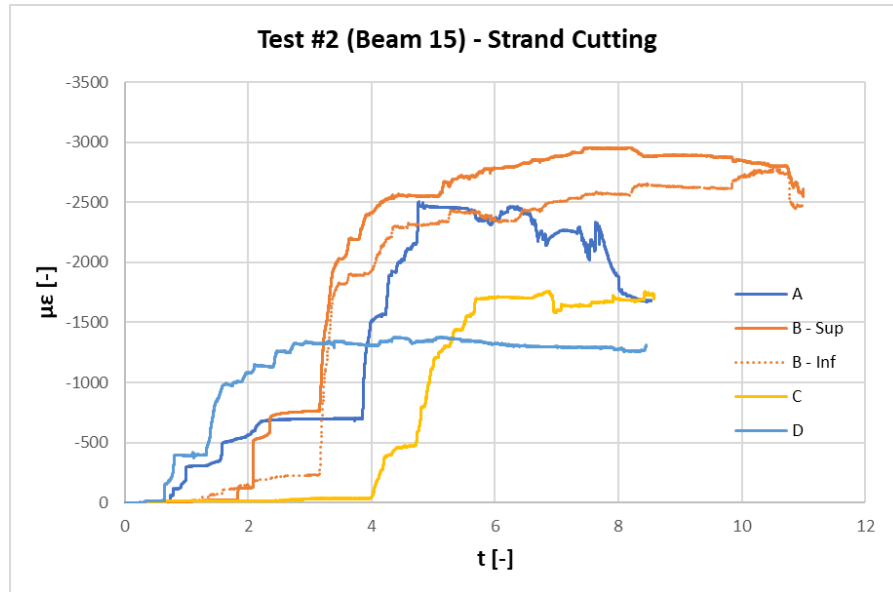
Figure 41. Strand cutting test measured strain on tested beam #2.

Beam	Point	Steel Strands Cut					
		z	z$_{real}$	με1	με2	σ$_{p1}$	σ$_{p2}$
		[m]	[m]	[-]	[-]	[N/mm^2]	[N/mm^2]
Test 2 - Beam 15	A	2.625	3.580	-1680.00	-	310.690	-
Code:	B	2.595	3.550	-2500.00	-2500.00	466.570	465.269
T8-P46/P47	C	14.795	15.750	-1700.00	-	314.304	-
	D	14.775	15.730	-1300.00	-	238.252	-

Table 5. Strand cutting test results for Beam #2.

A higher residual prestress value of 466.570 MPa is obtained in point B, both strain gauges in this point present readings of around 2500 micro-strains. The low values of stress obtained for points A, C, and D are dismissed.

Results beam #3, code T4-P46/P47.

Below are showcased the obtained strain reading for the concrete relax test and strand-cutting tests on tested beam #3. All concrete relax test readings were successful, for the strand-cutting test on point B the strain gauge detached when the strand was severed.
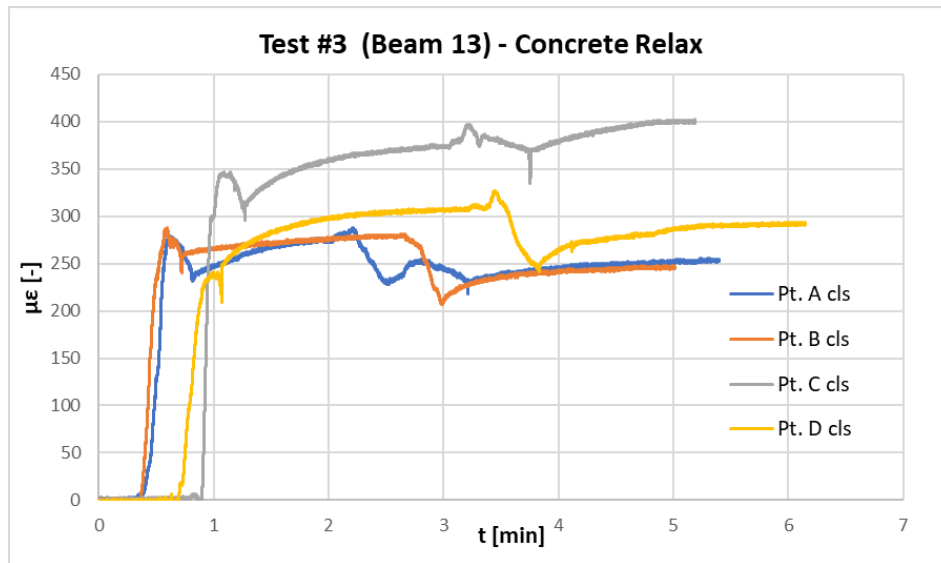
Figure 42. Concrete relax test measured strains on tested beam #3.
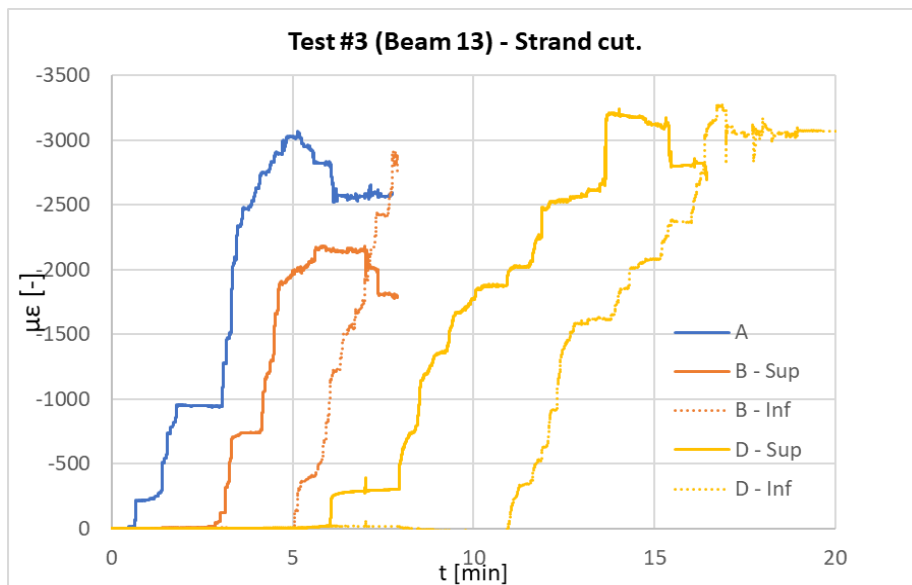
Figure 43. Strand cutting test measured strains on tested beam #3.

74

Beam	Point	Concrete Relax						
		z	z$_{real}$	Rck$_{media}$	με	σ$_{ps}$	σ$_{p1}$	σ$_{p2}$
		[m]	[m]	[N/mm^2]	[-]	[N/mm^2]	[N/mm^2]	[N/mm^2]
Test 3 - Beam 13	A	1.670	2.945	39.2	250	910.567	907.424	907.239
Code:	B	1.060	2.335	39.2	250	901.351	899.325	899.205
T4-P46/P47	C	7.000	8.455	39.2	400	1481.304	1473.320	1472.851
	D	7.000	8.455	39.2	295	1109.762	1101.778	1101.309

Table 6. Concrete relaxing test results for Beam #3.

Beam	Point	Steel Strands Cut					
		z	z$_{real}$	με1	με2	σ$_{p1}$	σ$_{p2}$
		[m]	[m]	[-]	[-]	[N/mm^2]	[N/mm^2]
Test 3 - Beam 13	A	1.805	3.080	-2590.00	-	490.833	-
Code:	B	1.755	3.030	-1700.00	-2700.00	321.758	511.566
T4-P46/P47	C	6.855	8.310	-	-	-	-
	D	7.035	8.490	-2800.00	-3070.00	529.000	579.836

Table 7. Strand cutting test results for Beam #3.

For this beam, the obtained results on the concrete relax test are similar between them, except for point C which presents a value too high. On the strand-cutting test, the lowest value is obtained by both strain gauges on point B, around 319 MPa, this value is dismissed.

Results beam #4, code T9-P46/P47.

On the concrete relax test, the obtained data on the concrete relax test on point B is 1050 micro-strains, which is significantly higher than the value obtained on the other three points, and it can be dismissed. For the steel cut test, there is correct data obtained for all four points except point C.
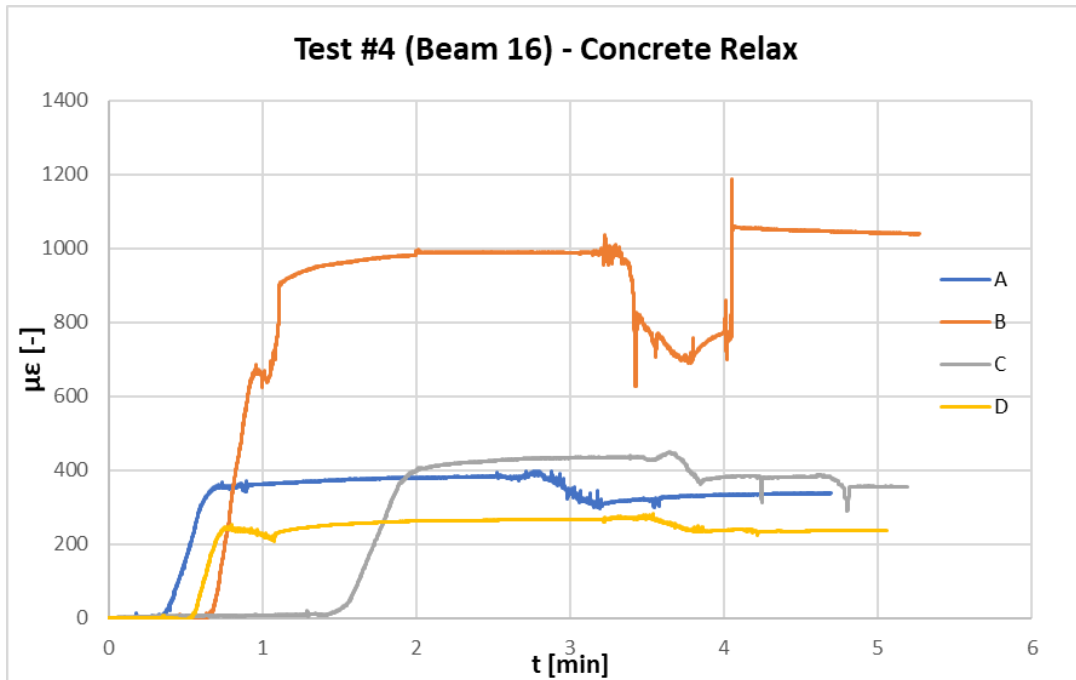
Figure 44. Concrete relax test measured strains on tested beam #4.
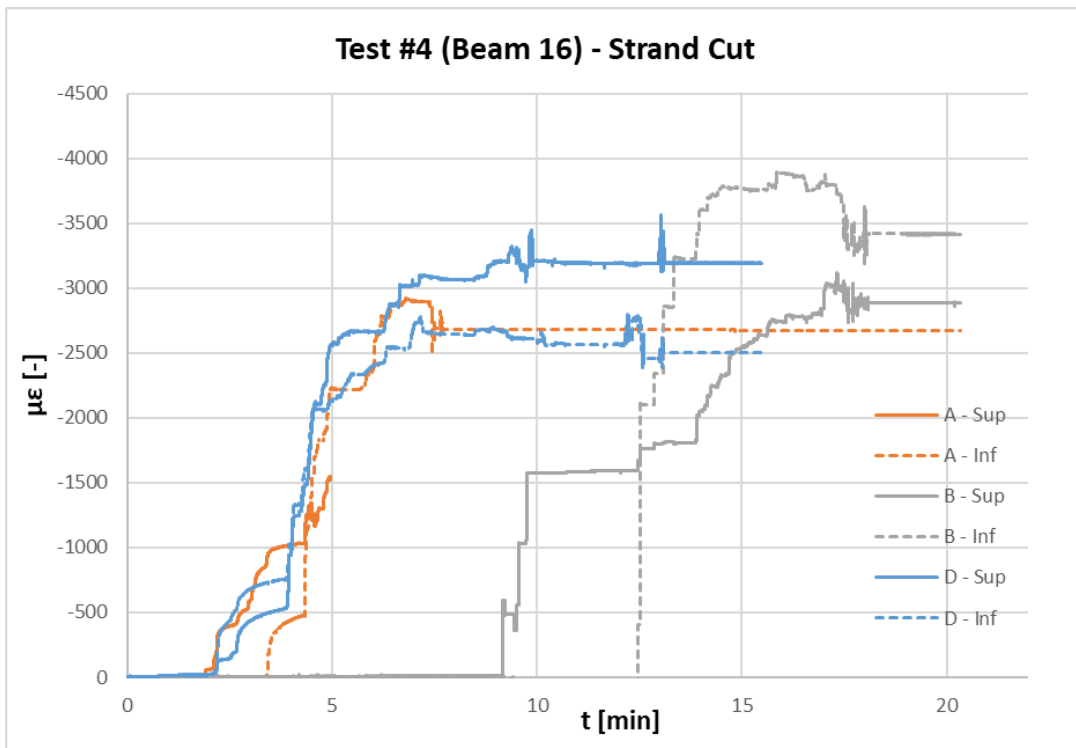
Figure 45. Strand cutting test measured strains on tested beam #4.

Beam	Point	Concrete Relax						
		z	z_{real}	Rck_{media}	$\mu\varepsilon$	σ_{ps}	σ_{p1}	σ_{p2}
		[m]	[m]	[N/mm^2]	[-]	[N/mm^2]	[N/mm^2]	[N/mm^2]
Test 4 – Beam 16	A	1.735	3.035	43	340	1071.888	1069.222	1069.065
Code:	B	4.835	6.135	43	1050	2633.241	2632.018	2632.018
T9-P46/P47	C	3.535	4.715	43	350	1154.638	1144.880	1144.306
	D	6.635	7.815	43	240	803.353	795.073	794.586

Table 8. Concrete relaxing test results for Beam #4.

Beam	Point	Steel Strands Cut					
		z	z_{real}	$\mu\varepsilon1$	$\mu\varepsilon2$	σ_{p1}	σ_{p2}
		[m]	[m]	[-]	[-]	[N/mm^2]	[N/mm^2]
Test 4 - Beam 16	A	1.735	3.035	-1523.00	-2670.00	287.784	506.127
Code:	B	4.835	6.135	-2890.00	-3400.00	548.634	645.462
T9-P46/P47	C	3.535	4.715	-	-	-	-
	D	6.635	7.815	-2500.00	-3190.00	471.846	602.459

Table 9. Strand cutting test results for Beam #4.

On the concrete relax tests, the computed remaining prestress values for points A and C are similar, around 1100 MPa, on point D a lower value is obtained, circa 645 MPa. The 2600 MPa obtained for point B are dismissed, this value makes no sense as it is higher than the initial prestressing on the strands. For the strand-cutting test, the lower values are obtained on point A, 287 MPa for both strands.

Results beam #5, code T7-P46/P47.

On beam #5 the strain values obtained on the concrete relax test are scattered between a minimum of 50 micro-strains and a maximum of 200 micro-strains, point D had a value of 670 micro-strains and is dismissed. For the strand cutting test are presented the values of points C, D, and F, missing points were either not instrumented or the strain gauge failed on the cutting.
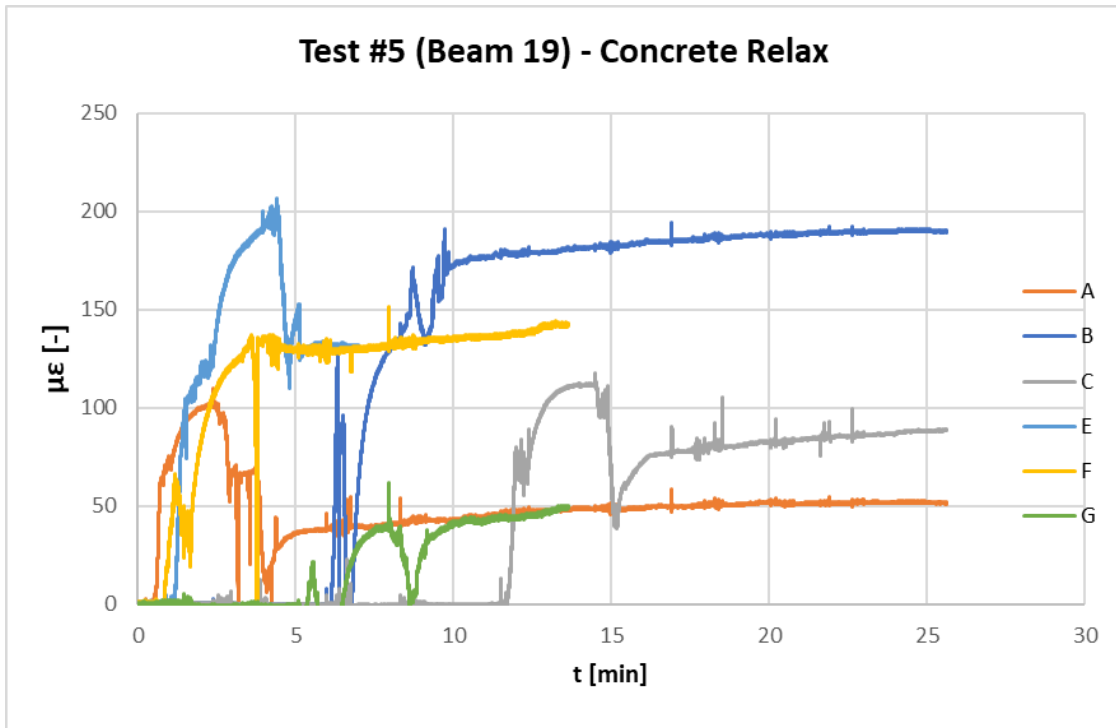
Figure 46. Concrete relax test measured strains on tested beam #5.
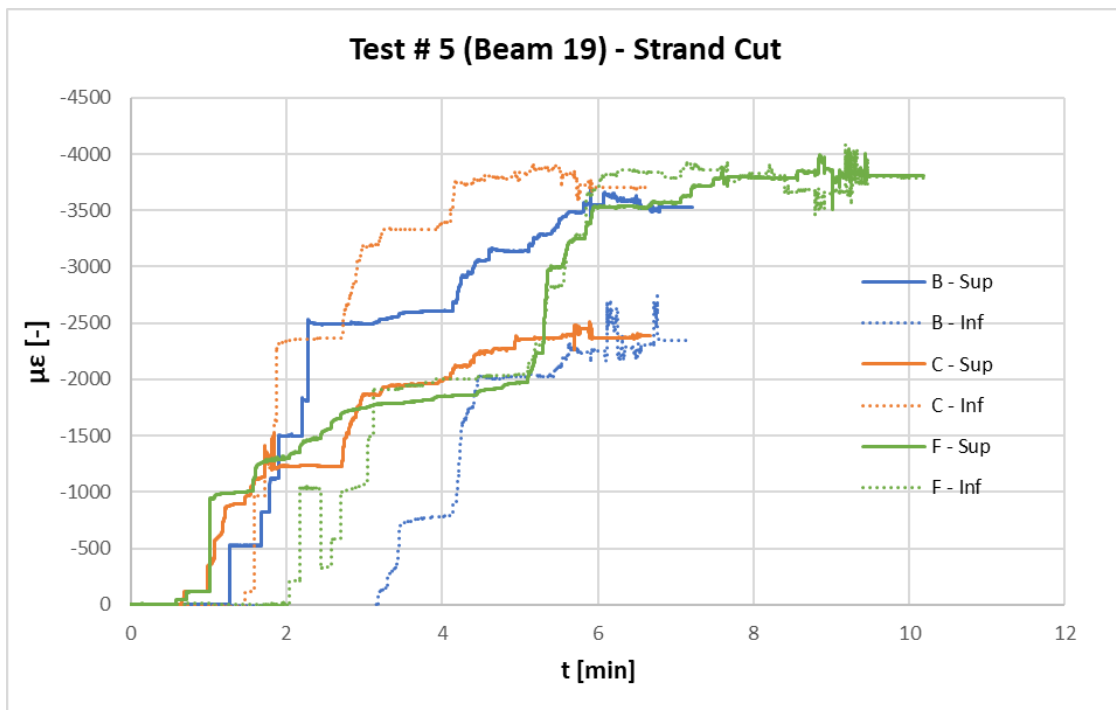
Figure 47. Strand cutting test measured strains on tested beam #5.

Beam	Point	Concrete Relax						
		z	z_{real}	Rck_{media}	$\mu\varepsilon$	σ_{ps}	σ_{p1}	σ_{p2}
		[m]	[m]	[N/mm²]	[-]	[N/mm²]	[N/mm²]	[N/mm²]
Test 5 - Beam 19	A	1.335	2.000	50.2	50	297.098	284.880	284.161
Code:	B	2.335	3.000	50.2	200	934.603	914.533	913.353
T7-P46/P47	C	4.335	5.000	50.2	100	569.711	537.279	535.371
	D	5.335	6.000	50.2	670	1980.203	1943.260	1941.087
	E	6.835	7.500	50.2	130	599.989	558.369	555.921
	F	12.885	13.550	50.2	140	584.947	549.896	547.834
	G	15.885	16.550	50.2	50	336.365	319.690	318.710

Table 10. Concrete relaxing test results for Beam #5.

Beam	Point	Steel Strands Cut					
		z	z_{real}	$\mu\varepsilon1$	$\mu\varepsilon2$	σ_{p1}	σ_{p2}
		[m]	[m]	[-]	[-]	[N/mm²]	[N/mm²]
Test 5 - Beam 19	A	1.365	2.030	-	-	-	-
Code:	B	2.365	3.030	-3500.00	-2350.00	657.261	437.568
T7-P46/P47	C	4.205	4.870	-3700.00	-2390.00	690.884	440.115
	D	5.565	6.230	-	-	-	-
	E	- -		-	-	-	-
	F	12.885	13.550	-3800.00	-3800.00	708.630	706.568
	G	- -		-	-	-	-

Table 11. Strand cutting test results for Beam #5.

On point A are found the lowest values for the concrete relax test, around 290 MPa; and the highest result of 1980 MPa on point D, all these three values are dismissed. For the six installed strain gauges were obtained values between 650 and 710 MPa.

Results beam #6, code T6-SP/P47.

On beam #6 there was only performed the concrete relax test. The results are shown below.
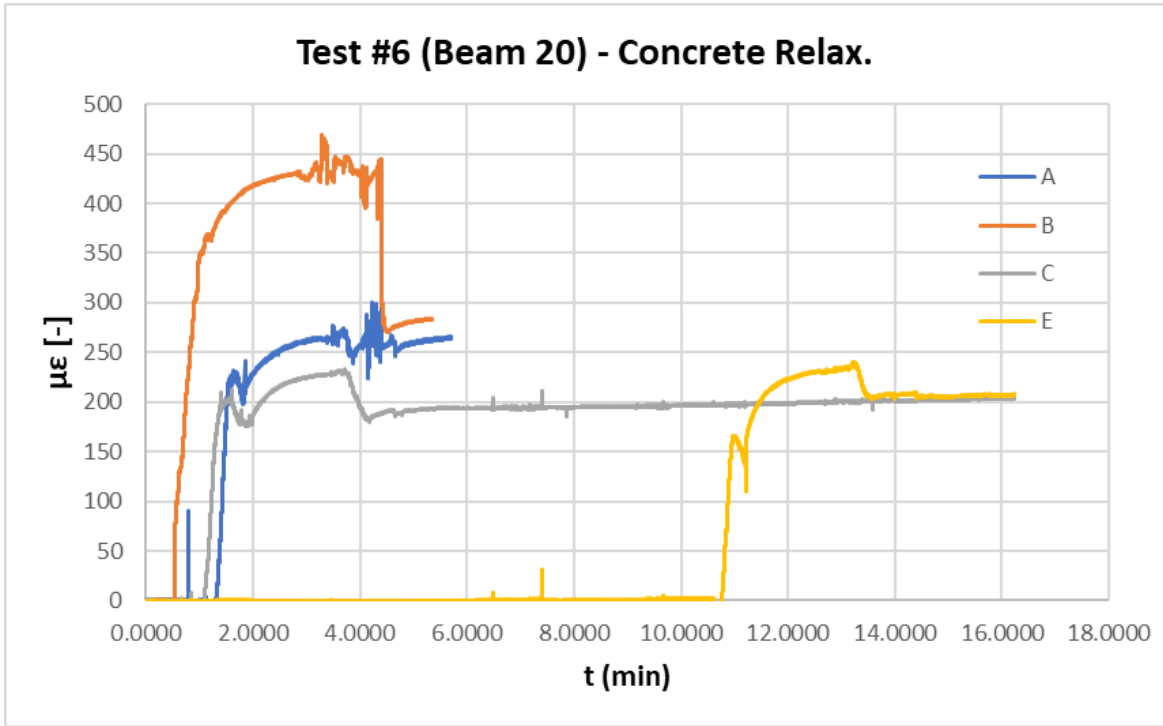
Figure 48. Concrete relax test measured strains, tested beam #6.

Beam	Point	Concrete Relax						
		z	z_{real}	Rck_{media}	$\mu\varepsilon$	σ_{ps}	σ_{p1}	σ_{p2}
		[m]	[m]	[N/mm²]	[-]	[N/mm²]	[N/mm²]	[N/mm²]
Test 6 - Beam 20	A	2.125	3.000	45.4	260	1118.779	1100.048	1098.946
Code:	B	5.125	6.000	45.4	290	958.176	921.809	919.670
T6-SP/P47	C	8.125	9.000	45.4	200	774.392	730.704	728.134
	D	12.625	13.500	45.4	-	-	-	-
	E	15.625	16.500	45.4	200	881.760	864.886	863.893

Table 12. Concrete relaxing test results for Beam #6.

In this case, the lowest obtained value is on point C, around 750 MPa; and the higher value is on point A, around 1105 MPa.

Summary.

The results for both types of tests on all 6 beams are summarized in Table 13. There are excluded the values commented in the previous section with clear measurement errors.

Beam	Point	Concrete Relax				Steel strands cut				
		με [-]	σcp1 [N/mm²]	σcp2 [N/mm²]	Mean σps [N/mm²]	με1 [-]	με2 [-]	σsp1 [N/mm²]	σsp2 [N/mm²]	Mean σp [N/mm²]
Test 1 - Beam 8	A	300.000	1116.061	1115.892	1115.977	-	-	-	-	-
Code:	A'	150.000	570.017	569.838	569.928	-	-	-	-	-
T3-P46/P47	B	300.000	730.596	730.869	730.732	-	-	-	-	-
	C	150.000	568.817	568.648	568.733	-	-	-	-	-
Test 2 - Beam 15	A	-	-	-	-	-	-	-	-	-
Code:	B	-	-	-	-	-2500.000	-2500.000	466.570	465.269	465.920
T8-P46/P47	C	-	-	-	-	-	-	-	-	-
Test 3 - Beam 13	A	250.000	907.424	907.239	907.332	-2590.000	-	490.833	-	490.833
Code:	B	250.000	899.325	899.205	899.265	-	-2700.000	-	511.566	511.566
T4-P46/P47	D	295.000	1101.778	1101.309	1101.544	-2800.000	-3070.000	529.000	579.836	554.418
Test 4 - Beam 16	A	340.000	1069.222	1069.065	1069.143	-	-2670.000	-	506.127	506.127
Code:	B	-	-	-	-	-2890.000	-3400.000	548.634	645.462	597.048
T9-P46/P47	C	350.000	1144.880	1144.306	1144.593	-	-	-	-	-
	D	240.000	795.073	794.586	794.830	-2500.000	-3190.000	471.846	602.459	537.153
Test 5 - Beam 19	B	200.000	914.533	913.353	913.943	-3500.000	-2350.000	657.261	437.568	547.414
Code:	C	100.000	537.279	535.371	536.325	-3700.000	-2390.000	690.884	440.115	565.500
T7-P46/P47	E	130.000	558.369	555.921	557.145	-	-	-	-	-
	F	140.000	549.896	547.834	548.865	-3800.000	-3800.000	708.630	706.568	707.599
Test 6 - Beam 20	A	260.000	1100.048	1098.946	1099.497	-	-	-	-	-
Code:	B	290.000	921.809	919.670	920.740	-	-	-	-	-
T6-SP/P47	C	200.000	730.704	728.134	729.419	-	-	-	-	-
	D	-	-	-	-	-	-	-	-	-
	E	200.000	864.886	863.893	864.389	-	-	-	-	-

Table 13. Results summary.

To compare the values, the following criteria are followed: for the points that there is data for both strands of the strand-cutting test (σ_{sp1} and σs_{p2}), the mean value of these two is compared against the mean value of the prestress in both strands obtained in the concrete-relax test (σ_{cp1} and σc_{p2}). If there is only data for one of the strands on the strand-cutting test, such value is compared against the correspondent value of that point obtained on the concrete-relax test, e.g. on point A for beam 3, there is data only for the second strand, σ_{sp2}, so this value is compared against the data obtained for the corresponding strand on the concrete relax test, σ_{cp2}; these criteria are followed for all points where there is data for both typology of tests,

points where there is information for only one type of test are not accounted. Using the concrete relax test we obtain averages values starting from a strain measurement on the concrete's surface, from which the stresses on each strand are computed using Navier's formula, the strand cut is a punctual test where the stresses are obtained directly for each strand, so averaging the values of both strands for each point it is obtained higher compatibility for both tests on each individual point of the beam. The comparison between the results is presented in table 14.

Beam	Point	Concrete Relax			Steel strands cut			Comparison		
		σ_{p1} [N/mm²]	σ_{p2} [N/mm²]	Mean σ_{ps} [N/mm²]	σ_{p1} [N/mm²]	σ_{p2} [N/mm²]	Mean σ_{ps} [N/mm²]	σ_{pc} [N/mm²]	σ_{ps} [N/mm²]	$\Delta\sigma$ [%]
Test 3 - Beam 13	A	907.424	907.239	907.332	490.833	-	490.833	907.424	490.833	45.9%
Code:	B	899.325	899.205	899.265	-	511.566	511.566	899.205	511.566	43.1%
T4-P46/P47	D	1101.778	1101.309	1101.544	529.000	579.836	554.418	1101.544	554.418	49.7%
Test 4 - Beam 16	A	1069.222	1069.065	1069.143	-	506.127	506.127	1069.065	506.127	52.7%
T9-P46/P47	D	795.073	794.586	794.830	471.846	602.459	537.153	794.830	537.153	32.4%
Test 5 - Beam 19	B	914.533	913.353	913.943	657.261	437.568	547.414	913.943	547.414	40.1%
Code:	C	537.279	535.371	536.325	690.884	440.115	565.500	536.325	565.500	-5.4%
T7-P46/P47	F	549.896	547.834	548.865	708.630	706.568	707.599	548.865	707.599	-28.9%
			SD (σps)	211.496		SD (σps)	67.738			

Table 14. Experimental residual prestress comparison.

For the concrete relax test, the maximum residual prestress found is 1101.54 MPa for point D on beam #3, and the lowest value is 536.325 MPa for point C of beam #5. For the strand-cut tests, the maximum value obtained was 707 MPa on point F of beam #5, while the lowest result is 490 MPa on point A of beam #3. The highest percentage variation obtained is 52.7 % for point A on beam #4 where the difference between the obtained results is 562.9 MPa, the highest agreement for both tests is achieved on point C of beam #5 with a prestress difference of 29.2 MPa and the lowest percent variation of 5.4%.

The results obtained from the concrete relax method are generally higher than the ones obtained from the strand cutting tests, but the first ones show a higher data scattering than the second ones, the variance for the concrete results is 211.5 MPa and for the strand cut tests is 67.7 MPa, the concrete-relax test is probably more

sensitive and the strand cutting test more robust causing such a difference in the results. The higher correspondence between the two types of tests is obtained on tested beam #5 which was not fully separated after the failure on the loading test.

Table 15 shows the theoretical values from the original designs (Ufficio Tecnico Lavori Publici - Città Di Torino, 1970). Table 16 compares the obtained values with the theoretical ones.

Initial theo. σp [N/mm²]	Residual theo. σp [N/mm²]	Theo. Loss σ$_p$ [N/mm²]	Prestress loss [%]
1400.77	836.3	564.47	40%

Table 15. Theoretical residual prestress and prestress loss.

Beam	Point	C. Relax			Strand Cut		
		σ$_{pc}$ [N/mm²]	σp Loss [N/mm²]	σp Loss [%]	σ$_{ps}$ [N/mm²]	σ$_p$ Loss [N/mm²]	σ$_p$ Loss [%]
Test 3 - Beam 13	A	907.424	493.346	35.2%	490.833	909.937	65.0%
Code:	B	899.205	501.565	35.8%	511.566	889.204	63.5%
T4-P46/P47	D	1101.544	299.226	21.4%	554.418	846.352	60.4%
Test 4 - Beam 16	A	1069.065	331.705	23.7%	506.127	894.643	63.9%
T9-P46/P47	D	794.830	605.940	43.3%	537.153	863.617	61.7%
Test 5 - Beam 19	B	913.943	486.827	34.8%	547.414	853.356	60.9%
Code:	C	536.325	864.445	61.7%	565.500	835.270	59.6%
T7-P46/P47	F	548.865	851.905	60.8%	707.599	693.171	49.5%

Table 16. Experimental prestress loss comparison.

In table 16 it can be seen that the higher prestress loss estimated using the concrete relax test is 61.8% which corresponds to 864.5 MPa, on point C for tested beam #5; the lowest loss registered is 21.4% corresponding to 299.23 MPa on point D on tested beam #3. For the strand-cutting test higher prestress loss is 65% which corresponds to 909.94 MPa on point A of beam 3, the lowest prestress loss is 49.5% registered on point F on tested beam #5. As mentioned before, on tested beam #5 is where a higher agreement is achieved reaching prestress losses of around 60% on both tests on all points except two lectures.

Compared to the theoretical value of 836.3 MPa of the residual stress and 40%

prestress losses, the strand-cutting method shows higher differences, but this theoretical value cannot be taken as a definitive reference as there is no verified information about the real residual stress on the strands after its tensioning. Destructive methods, such as cracking moment and decompression load tests, will provide further reference values to estimate prestress loss. Furthermore, the mechanical tests will provide more reliable material properties to be used in the presented methodologies.

6. Conclusions.

The end of design life for prestressed concrete infrastructure such as bridges built in the decade of the 70 represents an important consideration point for developed countries as not enough attention and resources are being allocated to the research and retrofitting of the current state of such structures. Existing structures are continuously exposed to detrimental factors such as aging, deterioration process, cyclic load, increasing applied load, impacts and accidents, improper working drainage systems, and bad or null maintenance, among others; such processes reduce the designed service life of the structure and may lead to an unexpected and catastrophic failure, as it has happened before. Assessing the current state of civil infrastructure via diagnostic tests is a vital process in preventing possible disasters in the future, safety tests can give engineers valuable information about the actual condition and properties and help them take decisions and actions about possible interventions.

In the present work has studied the prestress loss on 50-year-old precast prestressed concrete beams taken from the Corso Grosseto Viaduct. Two different methods have been considered: a non-destructive method named concrete relaxing test and a destructive method named strand cut test. The latter has been considered as a reference method to assess the concrete relaxing test as a method to be used on

existing structures. The concrete-relax test measures the strains on a small concrete block while it is detached from the bottom flange of a beam element, knowing these strains, Navier's equation can be used to determine the stress state on prestressed steel strands. The steel-cut test measures the compressive strains on a prestressed steel strand after being cut, the strand is first removed from all its concrete cover to install the strain gauge and perform the cut, the measured strains can be directly related to the residual prestress level on the strand.

Regarding the concrete relax test is possible to conclude that it is a promising methodology with clear advantages when it comes to replicability and performance in existing prestressed concrete members; it requires relatively simple equipment and not a specific-trained workforce, and it involves minimum section damage which can be easily repaired through the addition of new concrete in the point of the performed test. More accurate results for the concrete relax tests should be obtained when using the proper mechanical properties of the materials, as in this study are used the theoretical values obtained from the hammer rebound test and the Eurocode formulas.

The prestress loss obtained with the concrete relax method varies from 21.4% to 61.7%, while the ones obtained from the strand cutting test vary from 49.5% to 65%, the theoretically estimated losses presented on the original beam designs are 40%. The concrete relax test presents loss values closer to the theoretical one, but this theoretical value cannot be considered as a reference as it was not measured the actual prestress levels after the bridge construction. The variance for the data obtained on both tests are 211.5 MPa for the concrete relax test and 67.7 MPa for the steel-cutting test; the concrete relax test may have a higher sensibility compared to the robustness of the strand-cutting method which measures strains directly from the steel strands.

The strand-cutting test is a convenient methodology to directly measure the residual prestress force in prestressed steel strands. Its appliance requires higher manual

labor than the concrete relax test and does not require heavy machinery use. As it involves concrete cover and normal steel reinforcement removal, as well as the prestressed steel cutting, the PC element is irremediably damaged and should be considered as a destructive test not replicable in members still in use. For future research, it is important to procure a correct adherence of the strain gauge to the steel wire and assure to minimize the chance of harming it when the steel strand is cut.

In previous research strand cutting test has shown higher prestress loss readings, these are attributed to the possible influence of the concrete removal on local prestress losses and the violence of the strand cutting in the strain readings.

Future cracking moment and decompression load tests inside the BRIDGE|50 project along with more concrete relax and strand-cutting tests in the remaining beams will help establish the validity of these data.

7. References.

Anghileri, M., Biondini, F., Rosati, G., Savino, P., Tondolo, F., Sabia, D., Manto, S., Nivriera, M., Trincianti, C., Ventura, D., Monti, G., Legramandi, C., & Caruso, C. (2021). Deconstruction of the Corso Grosseto viaduct and setup of a testing site for full scale load tests. *Bridge Maintenance, Safety, Management, Life-Cycle Sustainability and Innovations - Proceedings of the 10th International Conference on Bridge Maintenance, Safety and Management, IABMAS 2020*, 3365–3370. https://doi.org/10.1201/9780429279119-457

Anghileri, M., Savino, P., Capacci, L., Bianchi, S., Rosati, G., Tondolo, F., & Biondini, F. (2021). *Non Destructive Testing and Model Validation of Corroded PC Bridge Deck Beams*. http://www.bridge50.org

Azizinamini, A., Keeler, B. J., Rohde, J., & Mehrabi, A. B. (1996). *Application of a New Nondestructive Evaluation Technique to a 25-Year-Old Prestressed Concrete Girder*.

Bagge, N., Nilimaa, J., & Elfgren, L. (2017). In-situ methods to determine residual prestress forces in concrete bridges. *Engineering Structures*, *135*, 41–52. https://doi.org/10.1016/j.engstruct.2016.12.059

Baran, E., Shield, C. K., & French, C. (2015). *A Comparison of Methods for Experimentally Determining Prestress Losses in Pretensioned Prestressed Concrete Girders*. https://www.researchgate.net/publication/262057133

Biondini, F., Manto, S., Beltrami, C., Tondolo, F., Chiara, M., Salza, B., Tizzani, M., Chiaia, B., Lencioni, A., Panseri, L., & Quaranta, L. (2021). BRIDGE|50 research project: Residual structural performance of a 50-year-old bridge. *Bridge Maintenance, Safety, Management, Life-Cycle Sustainability and Innovations - Proceedings of the 10th International Conference on Bridge Maintenance, Safety and Management, IABMAS 2020*, 3337–3344. https://doi.org/10.1201/9780429279119-453

Biondini, F., Tondolo, F., Manto, S., Beltrami, C., Chiara, M., Salza, B., Tizzani, M., Chiaia, B., Lencioni, A., Panseri, L., & Quaranta, L. (2021). *Residual Structural Performance of Existing PC Bridges: Recent Advances of the BRIDGE|50*

Research Project.

Bonopera, M., Chang, K.-C., & Lee, Z.-K. (2020). State-of-the-Art Review on Determining Prestress Losses in Prestressed Concrete Girders. *Applied Sciences*, *10*(20), 7257. https://doi.org/10.3390/app10207257

Bruce, S. M., McCarten, P. S., Freitag, S. A., & Hasson, L. M. (2008). *Deterioration of prestressed concrete bridge beams*. Land Transport New Zealand.

Civjan, S. A., Jirsa, J. 0, Carrasquillo, R. L., & Fowler, D. W. (1998). *Instrument to Evaluate Remaining Prestress in Damaged Prestressed Concrete Bridge Girders.*

de Schutter, Geert. (2013). *Damage to concrete structures*. Taylor & Francis.

E. C. (2005). *EN 1992-1-1: Eurocode 2: Design of concrete structures - Part 1-1: General rules and rules for buildings.*

Fontana, M. G. (1987). *Corrosion Engineering* (S. Rao, Ed.; International). McGraw-Hill.

Frizzarin, M., Faleschini, F., Zanini, M. A., Franchetti, P., & Pellegrino, C. (2019). *Experimental detection of the residual prestressing level in pre-tensioned and post-tensioned reinforced concrete beams by means of non-destructive tests.*

Garber, D. B., Gallardo, J. M., Deschenes, D. J., & Bayrak, O. (2015). Experimental investigation of prestress losses in full-Scale bridge girders. *ACI Structural Journal*, *112*(5), 553–564. https://doi.org/10.14359/51687909

Halsey, J. T., & Miller, R. (1996). *Destructive Testing of Two Forty-Year-Old Prestressed Concrete Bridge Beams.*

Hamilton, T., West, J., Wouters, J., & American Concrete Institute (ACI). (2005). *ACI 222.2R-01 Corrosion of Prestressing Steels.*

Higgs, A., Barr, P. J., & Halling, M. W. (2015). Comparison of Measured and AASHTO LRFD-Predicted Residual Prestress Forces, Shear and Flexural Capacities of High-Strength Prestressed-Concrete Bridge Girders. *Journal of Bridge Engineering*, *20*(1). https://doi.org/10.1061/(asce)be.1943-5592.0000646

Kukay, B., Barr, P. J., Halling, M. W., & Womack, K. (2010). *Determination of the Residual Prestress Force of In-Service Girders using Non- Destructive Testing.*

Kukay, B. M. (2008). *Bridge Instrumentation and the Development of Non-Destructive and Destructive Techniques Used to Estimate Residual Tendon Stress in Prestressed Girders*. https://digitalcommons.usu.edu/etd/128

Labia, Y., Saiidi, M. S., & Douglas, B. (1997). Full-Scale Testing and Analysis of 20-Year-Old Pretensioned Concrete Box Girders Title no. 94-S43. In *ACI Structural Journal* (Vol. 94, Issue 5).

Lau, K., & Lasa, I. (2016). Corrosion of prestress and post-tension reinforced-concrete bridges. In *Corrosion of Steel in Concrete Structures* (pp. 37–57). Elsevier Inc. https://doi.org/10.1016/B978-1-78242-381-2.00003-1

Maya Vélez, D., Corrado, M., & Ventura, G. (2019). *Influence of the existing stress state on the pull-out test for concrete structures*.

Onyemelukwe, O. U., & Mills, C. J. (2003). *Field Measured Pre-stress Concrete Losses Versus Design Code Estimates*.

Parrondo Rodriguez, J. (2017). El hundimiento del puente de la carretera M-527 sobre el río Guadarrama. *Revista de Obras Públicas: Organo Profesional de Los Ingenieros de Caminos, Canales y Puertos, 3583*, 74–95.

Podolny, W. (1992). *Corrosion of Prestressing Steels and Its Mitigation Long-time*.

Rogers, R. A., Wotherspoon, L., Scott, A., & Ingham, J. M. (2012). Residual strength assessment and destructive testing of decommissioned concrete bridge beams with corroded pretensioned reinforcement. *PCI Journal, Summer*, 100–118.

Savino, P., Anghileri, M., Chiara, M., Salza, B., & Quaranta, L. (2021). Corso Grosseto viaduct: Historical and technical overview. *Bridge Maintenance, Safety, Management, Life-Cycle Sustainability and Innovations - Proceedings of the 10th International Conference on Bridge Maintenance, Safety and Management, IABMAS 2020*, 3345–3351. https://doi.org/10.1201/9780429279119-454

Shenoy, C. v, & Frantz, G. C. (1991). *Structural Tests of 27-Year-Old Prestressed Concrete Bridge Beams*.

Tondolo, F., Biondini, F., Sabia, D., Gianpaolo, R., Chiaia, B., Quattrone, A., Savino, P., & Anghileri, M. (2021). *Experimental Program and Full-Scale Load Tests on PC Deck Beams*. www.bridge50.org

Ufficio Tecnico Lavori Publici - Città Di Torino. (1970). *Largo Grosseto, Intercambio Viale - Progetto Esecutivo.*

Woodward, R. J. (1989). *Collapse of a Segmental Post-Tensioned Concrete Bridge.*